An Initial Assessment of Data from the Advanced Technology Microwave Sounder

Forecast R&T Report no. 569

October 2012

Amy Doherty, Nigel Atkinson,
William Bell, Brett Candy,
Simon Keogh and Chelsey Cooper

If printing double sided you will need this blank page. If printing single sided, please delete this page.

Contents

Abstract

This initial assessment is based on an evaluation of ATMS data covering the period January - February 2012 as well as a small amount of near real time data received after 26th June 2012. ATMS data quality was assessed by examining observation minus background brightness temperature differences, or innovations, and comparing them to those for AMSU and MHS. The remapping of ATMS data at the Met Office achieves significant improvements in the effective radiometric performance of the data. For the key lower atmospheric sounding channels (6-10) the effective NEΔTs, derived from the on-orbit warm load views, are in the range 60-100 mK. This compares favourably with equivalent NEΔTs for AMSU-A which fall in the range 140-180 mK after processing by the ATOVS and AVHRR pre-processing package (AAPP). The *uncorrected* innovations for ATMS have similar statistical characteristics (mean and standard deviation) as AMSU / MHS. The presence of a striping effect in the innovation maps for the temperature sounding channels, increases the variance in the bias corrected innovations for ATMS to values higher than those for AMSU-A. The amplitude of these effects, at several tenths of a Kelvin, is sufficient to be a concern for NWP data assimilation applications so improvements in dealing with these effects are desirable over the coming months. When added to a full Met Office system in a 30 day assimilation experiment the impact of the ATMS observations is neutral, an encouraging result from these early experiments.

1. Introduction

The Polar Operational Environmental Satellite (POES) series of satellites have provided key data for Numerical Weather Prediction (NWP) since 1978. Microwave temperature sounding data has been provided by the Microwave Sounding Unit (MSU) carried onboard satellites launched during the period 1978-1994 and more recently by the Advanced Microwave Sounding Unit (AMSU) carried onboard POES, Metop and Aqua satellites launched during the period from 1998 – 2012 (Goodrum et al., 1999). One further AMSU instrument will be launched as part of the EUMETSAT's Metop series (Metop-C). Over the next decade, continuity of these important observations will be provided by instruments of the US-European Joint Polar Satellite System (JPSS) (Marburger, 2011). The US component of JPSS will use a new microwave sounding instrument developed by NASA - The Advanced Technology Microwave Sounder (ATMS) (Muth *et al.* 2004). ATMS is a cross track scanning microwave radiometer first flown on the preparatory mission of the JPSS series – the Suomi NPP satellite launched on 28th October 2011.

A sample data set covering the period 18th January to 18th February 2012 has been assessed at the Met Office and a near real time data stream to the Met Office was established on June 26th 2012. The aim of this report is to summarise the findings of this initial assessment of ATMS data using the Met Office global data assimilation system. The use of NWP data assimilation systems in the on-orbit characterisation of satellite sounding instruments is now well established (see Lu *et al*. 2011) and this approach has been very effective in detecting and correcting a range of systematic errors in instruments and in radiative transfer models.

ATMS is similar, but not identical, to the AMSU instruments flown on NOAA-15 to -19 and Metop-A. It has 22 channels: 5 sensitive to the surface, 11 temperature sounding channels around the 50-60 GHz oxygen band and 6 moisture sounding channels around

the 183 GHz water vapour band. Table 1 shows the channel characteristics of ATMS and details of AMSU channels where they correspond to ATMS.

ATMS has 96 footprints per scan line, each separated by 1.11º. The footprint size varies with channel. Channels 1 and 2 have a 5.2º footprint, channels 3-16 have a 2.2º footprint and channels 17-22 have a 1.1º footprint. This means that the lower frequency channels are highly oversampled.

The oversampling of the 50-60 GHz temperature sounding channels is accompanied by shorter integration times per footprint and results in higher radiometric noise values, relative to equivalent AMSU channels. In current operational data assimilation systems it is known that errors in the short range forecast fields, expressed as observation equivalent brightness temperatures, are typically in the range 0.05-0.10 K for mid-tropospheric temperature sounding channels. This places very demanding requirements on the performance of microwave sounding instruments, in terms of radiometric performance (Bell *et al.,* 2010) as well as systematic biases in the data.

Table 1. ATMS and AMSU channel characteristics. White rows show channels which are identical to AMSU, blue rows show channels where there is a change to polarisation or frequency, or both and green rows show the new channels on ATMS[i]

ATMS Channel number	AMSU Channel number	Centre Frequency (GHz)	Bandwidth (MHz)	Polarisation	Characterisation at nadir
1	1	23.8	258	V	window-water vapor
2	2	31.4	172	V	window-water vapour
3	3	50.3	173	H	window surface emissivity
4	-	51.76	381	H	window surface emissivity
5	4	52.8	366	H	Surface air
6	5	53.596 +/- 0.116	2x162	H	4 km ~ 700 mb
7	6	54.4	387	H	9 km ~ 400 mb
8	7	54.94	387	H	11 km ~ 250 mb
9	8	55.5	317	H	13 km ~ 180 mb
10	9	f0=57.29026+/- 0.087	2x151	H	17 km ~ 90 mb
11	10	f0+/- 0.217	2x76	H	19 km ~ 50 mb
12	11	f0 +/- 0.3222+/-0.048	4x35	H	25 km ~ 25 mb
13	12	f0 +/- 0.3222+/-0.022	4x15	H	29 km ~ 10 mb
14	13	f0 +/- 0.3222+/- 0.010	4x8	H	32 km ~ 6 mb
15	14	f0 +/- 0.3222+/-0.0045	4x3	H	37 km ~ 3 mb
16	15/16	88.2	1928	V	Window H2O
17	17	165.5 +/- 0.925	2x1125	H	H2O 18 mm
18	20	183.31 +/- 7.0	2x1930	H	H2O 18 mm
19	-	183.31 +/- 4.5	2x1952	H	H2O 4.5 mm
20	19	183.31 +/- 3.0	2x980	H	H2O 2.5 mm
21	-	183.31 +/- 1.8	2x982	H	H2O 1.2 mm
22	18	183.31 +/- 1.0	2x494	H	H2O 0.5 mm

At the Met Office the ATOVS and AVHRR Preprocessing Package (AAPP)[ii] is used to remap the data in order to bring them close to AMSU noise performance and footprint size (NWP SAF, 2011a). The ATMS data assessed here have been manipulated to a beam width of 3.3º (apart from channels 1 and 2 for which the beam width is 4.8º) and have been resampled to give one field of view in three across the scan (giving 32 fields of view across the scan). The data are also resampled at a rate of 1 in 3 in the along track direction.

The data quality has been assessed through analysis of innovations before and after bias correction, and of NEΔT values for the instrument. Comparison with AMSU is used to determine if the data quality is of an acceptable level. Section 2 presents the results of the comparison with AMSU together with a summary of the Met Office bias correction scheme. In Section 3 results of assimilation experiments are presented with reference to control experiments that represent closely the Met Office global assimilation system. Standard Met Office NWP trial metrics, such as the impact of the new instrument on the NWP index, are reported as well as changes to the background (T+6 hour forecast) fit to key observation types (AMSU, IASI and radiosondes) when the ATMS data are added.

2. Data Quality

2.1 Bias correction

A careful assessment of data quality is a critical first step towards the operational assimilation of any new satellite data. In addition to identifying channels with gross errors and developing screening tests for these channels, bias corrections are applied to correct for systematic errors (in instruments, radiative transfer modelling or the forecast model itself), which show up as persistent mean differences between the modelled and observed values of brightness temperature (O-B). Recent experience (Lu *et al.,* 2011) has shown that, for many temperature sounding channels on several instruments, the dominant biases are related to errors in

- Instrument characterisation
- Sub-optimal *on-orbit* performance
- Radiative transfer (RT) modelling errors

Except for near the model top where few observations exist, the errors are not usually in the short range forecast model fields themselves, which are initialised from analyses which are tightly constrained by a large and diverse range of observational data. The sensitivity of NWP based techniques in detecting such biases is estimated to be several tenths of a Kelvin.

After bias correction some differences, or *residual biases*, can remain and these are of interest in assessing the quality of the data that will be assimilated. The Met Office employs a *static* bias correction scheme, which is updated periodically. The bias model, (which aims to represent the form and magnitude of the biases) is based on the scheme of Harris & Kelly (2001). In this scheme, the modelled bias (ΔT_B) is represented as a sum of several terms:

$$\Delta T_B^{\,i,j} = c_0^{\,i} + c_1^{\,i,j} + c_2^{\,i} \int_{p=850hPa}^{p=300hPa} \frac{dp}{\rho(p)g} + c_3^{\,i} \int_{p=200hPa}^{p=50hPa} \frac{dp}{\rho(p)g} \qquad (1)$$

where:

i, j represent the indices for channel i, and field of view j.

$c_0^{\,i}$ represents a *global offset*, in Kelvin, for channel i.

$c_1^{\,i,j}$ represents a field of view (j) dependent offset, for channel i.

$c_2^{\,i}$ represents the coefficient of an *airmass* dependent term, representing in this case the thickness of an atmospheric layer between 850 – 300 hPa, in K.m^{-1}.

$c_3^{\,i}$ represents the coefficient of an *airmass* dependent term, representing in this case the thickness of an atmospheric layer between 200 – 50 hPa, in K.m^{-1}.

p represents pressure at a model level, and dp the pressure difference between adjacent model levels, in Pa.

ρ represents the mean density in an atmospheric layer, in kg.m^{-3}.

g represents acceleration due to gravity, in m.s^{-2}

The first term ($c_0^{\,i}$) accounts for gross instrument calibration errors in the data and removes much of the inter-satellite biases in microwave sounding data. The second term ($c_1^{\,i,j}$) accounts for variation in the bias across the track. Biases across the scan can be as large as ~1 K (Lu *et al*., 2010) and can result from intrusions into the radiometer field of view. Such intrusions often lead to strong scan asymmetries and typically affect the extreme fields of view of the scan. Radiative transfer modelling errors can also result in cross scan biases (Peubey, 2011), however, these normally result in symmetric cross scan biases. Other possible causes of cross-scan biases include cross-polarisation sensitivity, polarisation twist and non-ideal antenna reflectivity (NWP SAF, 2011b). The third and fourth terms in Equation 1 represent airmass dependent corrections and correct for the commonly observed latitudinal variations in biases. Such biases can result from radiative transfer modelling errors, instrument calibration errors or forecast model errors. A recent study of China's FY-3A Microwave Temperature Sounder (MWTS) (Lu *et al*., 2010) demonstrated that significant radiometer passband shifts can be manifested as airmass dependent biases. The coefficients c_0 to c_3 are determined by linear regression.

In summary the bias correction scheme described above is expected to reduce much of the stationary, or near stationary, structure in the fields of O-B. The subsections below assess the form of these uncorrected biases, and the effectiveness of the bias correction scheme in eliminating them.

2.2 Cross-track biases

Figure 2 shows the cross track biases for ATMS for chs 6-15, 18, 20 and 22. Means are plotted at the top with standard deviation below for each channel. Also plotted are the corresponding ATOVS channel means and standard deviation of biases from NOAA-18 and NOAA-19.

For ATMS channels 8-15 the variation of mean O-B is generally symmetric about the nadir view and varies smoothly across the scan, in most cases taking a near parabolic form. The variation across the scan is typically several tenths of a Kelvin from nadir to the edge of swath. This contrasts with the scan biases for AMSU-A which are more irregular across the swath. The standard deviation of the innovations across the swath is generally more consistent than for AMSU-A.

For channels 6 and 7 slight asymmetries exist across the swath for ATMS.

For the humidity sounding channels examined here (18, 20 and 22 corresponding to 183±7, ±3, ±1 GHz) cross scan biases show similar levels of asymmetry and irregularity as the AMSU-B equivalent channels on NOAA-18 and NOAA-19. The standard deviation of the innovations are consistent across the scan.

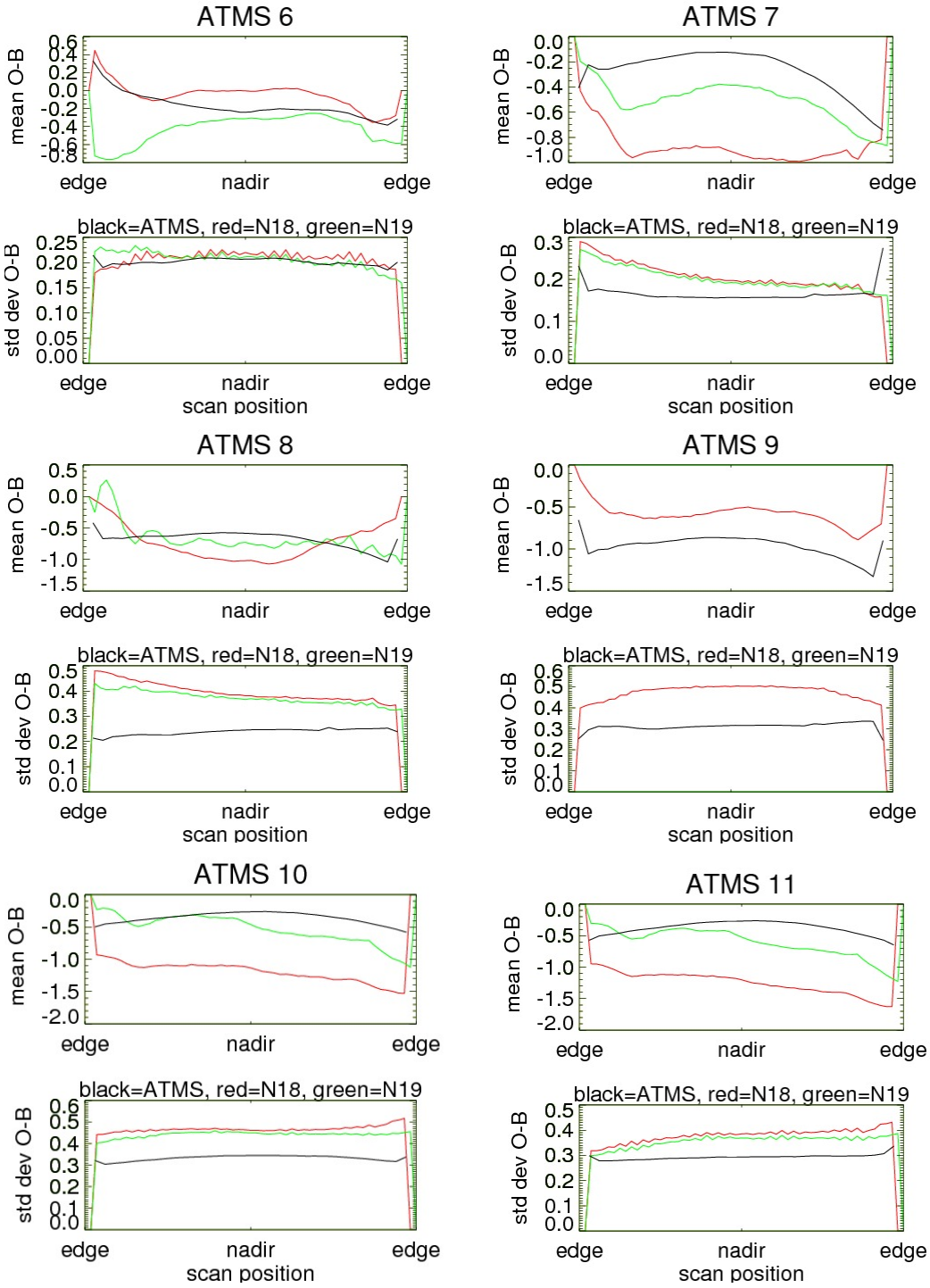

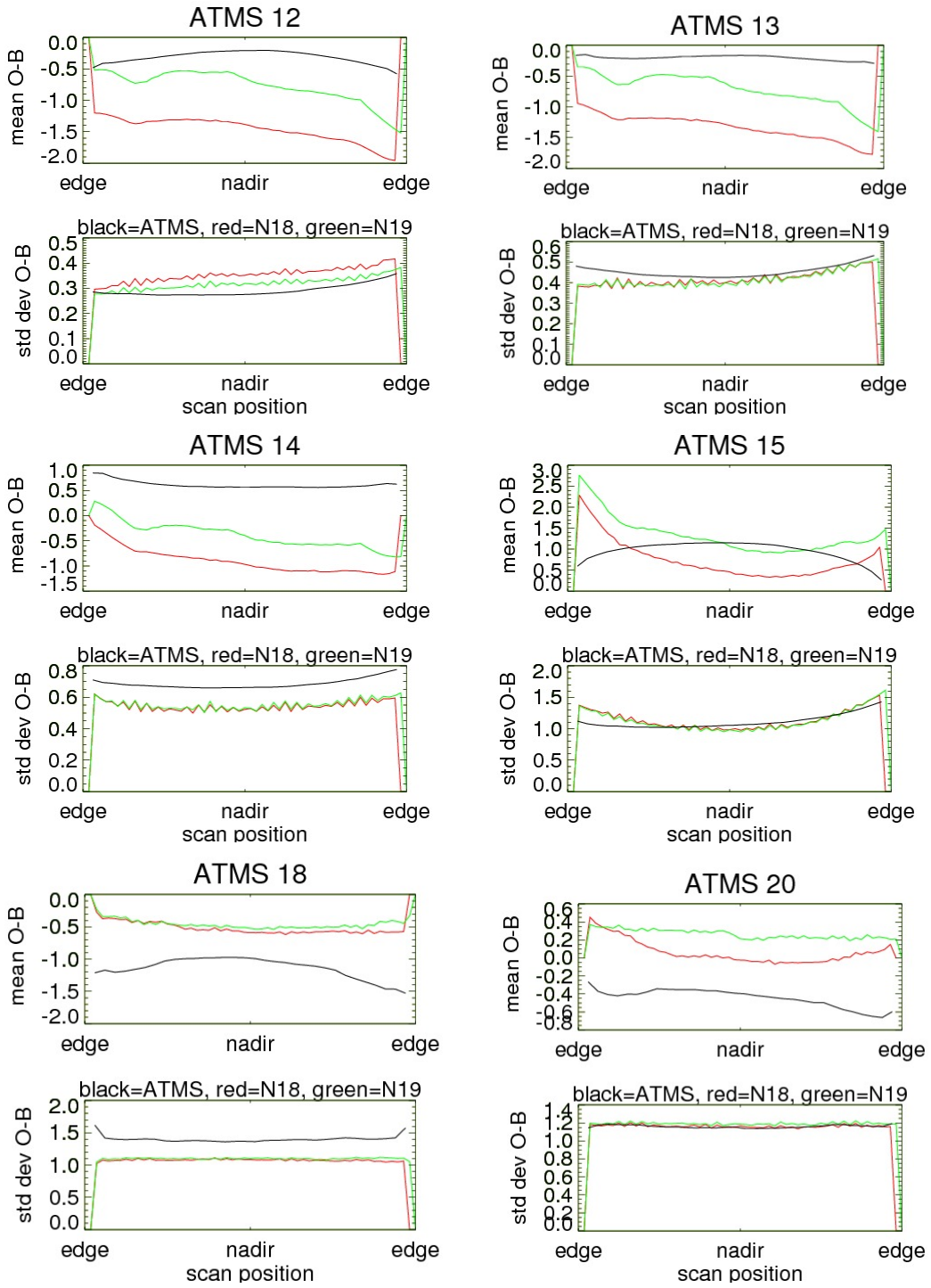

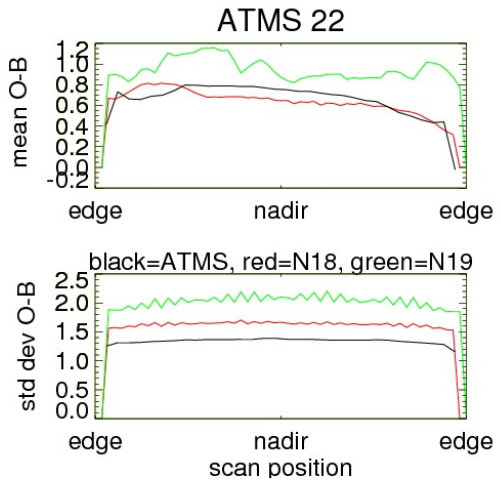

Figure 2: ATMS and ATOVS uncorrected cross track biases from Jan/Feb 2012 for ATMS channels 6-15 and 18, 20, 22.

2.3 Geographical distribution of biases

Figure 3 shows maps of uncorrected and corrected innovations (O-B and C-B) for ATMS channels 6-15 for the six hour assimilation cycle centred on 00Z on 30th July 2012. These maps are representative of other 6 hour periods examined, but not shown.

The asymmetric cross scan bias for channel 6 and 7, discussed in Section 2.2, are corrected effectively by the bias correction scheme. For channels 8-15 the dominant features in the uncorrected innovation maps are: (i) regular stripes of missing data, as a consequence of the fact that the AAPP spatial filtering is performed on blocks of 320 seconds and 3 scans at the edge of each block are discarded; and (ii) apparent airmass related bias. These airmass related biases show maximum O-B values at latitudes south of 50°S, are coherent across channels 8-15, and show an equator to southern polar region variation of approximately 0.5-2.5 K. There is inter-hemispheric asymmetry in the biases in that they are most evident in the southern polar regions and, although still evident in some channels (9-11), are much less pronounced at high northern latitudes.

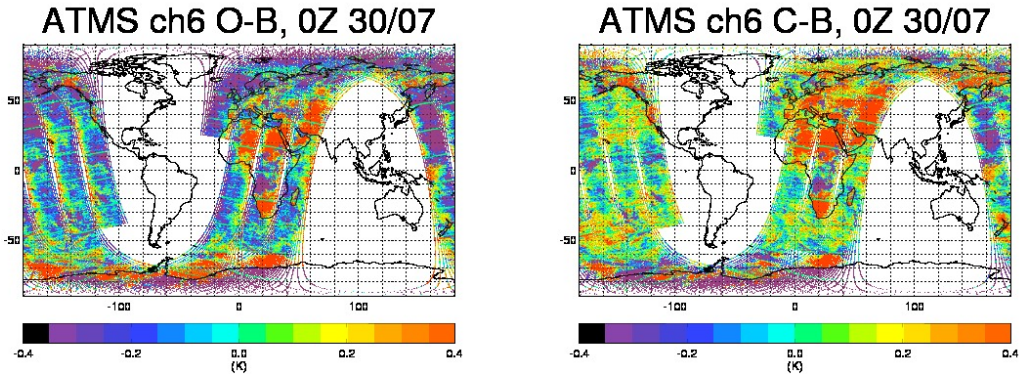

ATMS ch7 O-B, 0Z 30/07

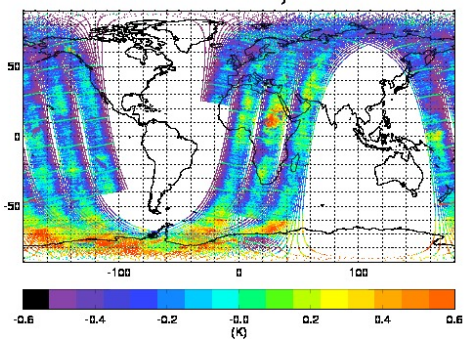

ATMS ch7 C-B, 0Z 30/07

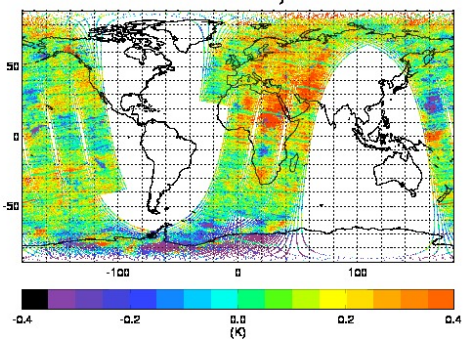

ATMS ch8 O-B, 0Z 30/07

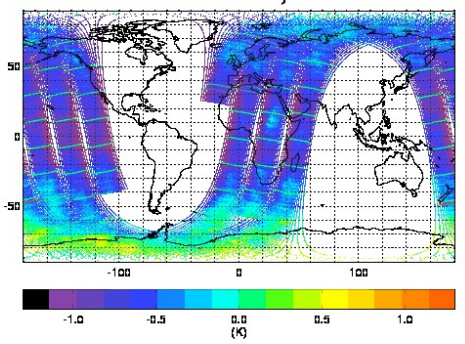

ATMS ch8 C-B, 0Z 30/07

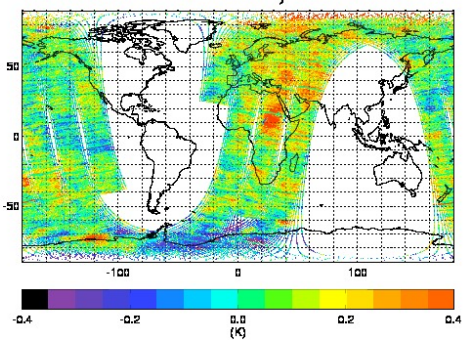

ATMS ch9 O-B, 0Z 30/07

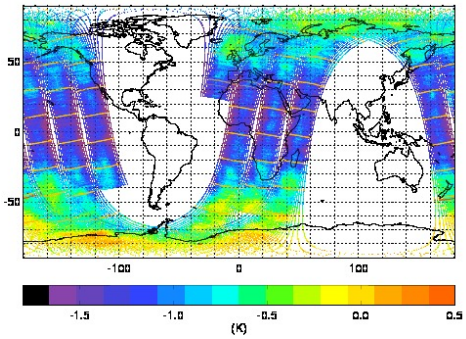

ATMS ch9 C-B, 0Z 30/07

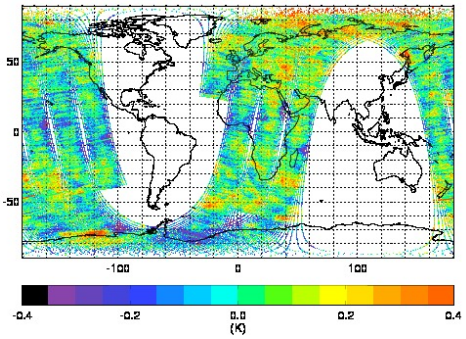

ATMS ch10 O-B, 0Z 30/07

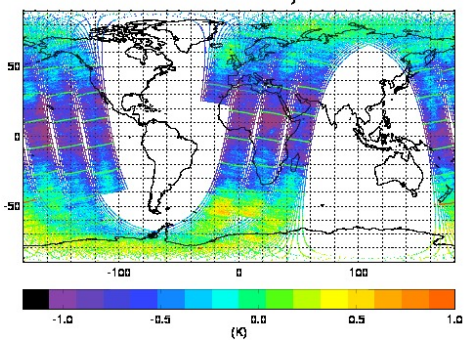

ATMS ch10 C-B, 0Z 30/07

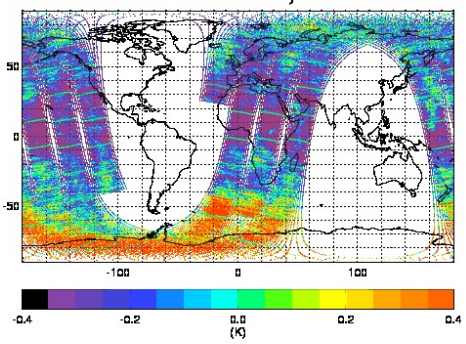

ATMS ch11 O-B, 0Z 30/07

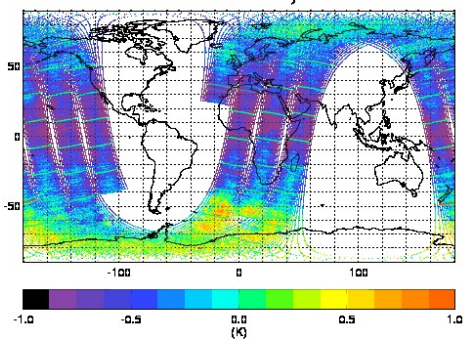

ATMS ch 11 C-B 0Z 30/07

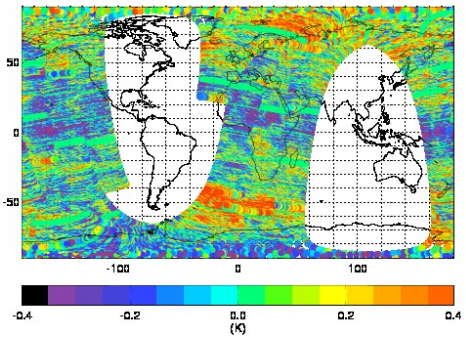

ATMS ch12 O-B, 0Z 30/07

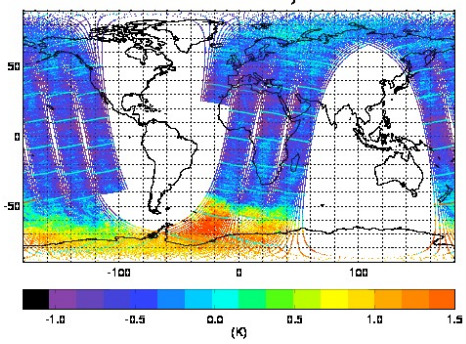

ATMS ch 12 C-B 0Z 30/07

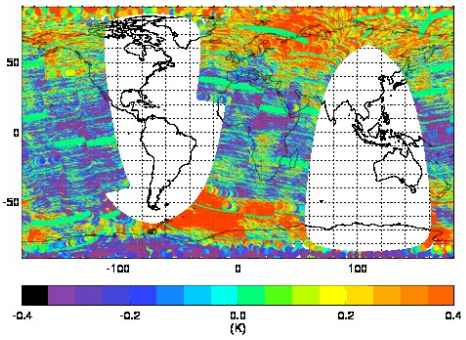

ATMS ch13 O-B, 0Z 30/07

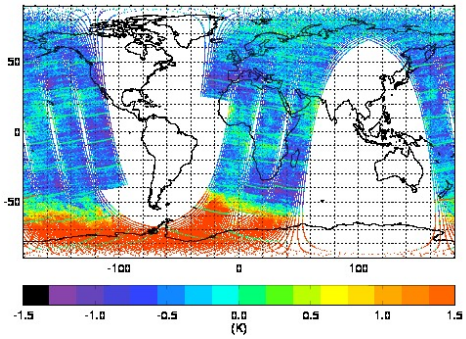

ATMS ch13 C-B, 0Z 30/07

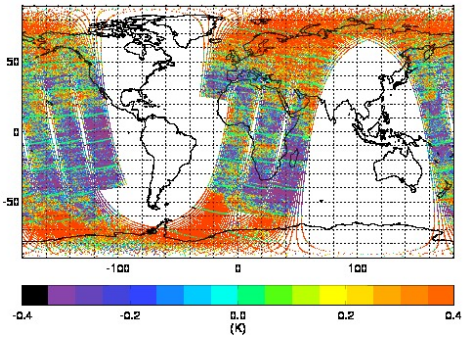

ATMS ch14 O-B, 0Z 30/07

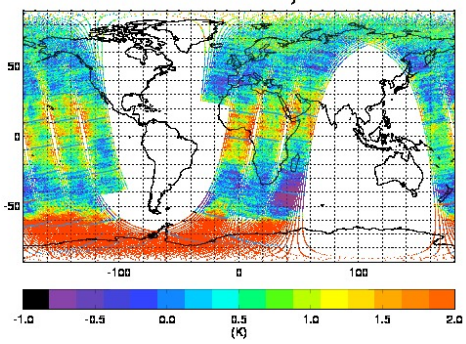

ATMS ch14 C-B, 0Z 30/07

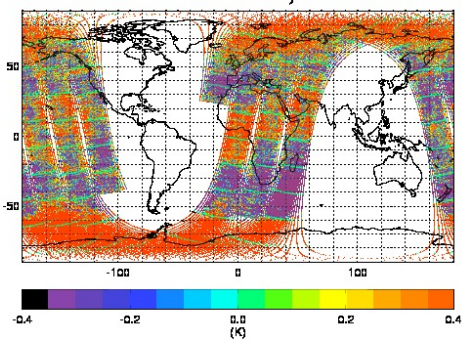

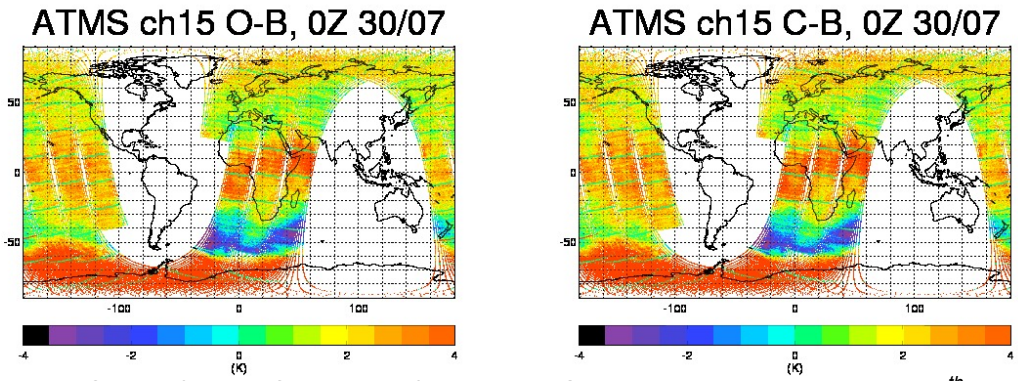

Figure 3: O-B (left) and C-B (right) for N19 AMSU channels 6-15 at 0Z on 30th July

The bias correction scheme is reasonably effective in reducing the variance of the O-Bs for the key tropospheric sounding channels (6-9). The variance is also reduced for the other channels, but significant local biases remain in channels 10-15, particularly associated the warm bias in the high southern latitudes which is only partially corrected. Generally the ATMS biases are lower than AMSU with the exception of channels 9, 18 and 22. The AMSU data does not show the same latitude dependent biases seen in the ATMS data. A warm bias is seen in the Southern Hemisphere in AMSU channels 12 and13 (ATMS 13 and 14) (Figure 4) but it is not as pronounced as for ATMS and in the other AMSU channels the bias is not seen.

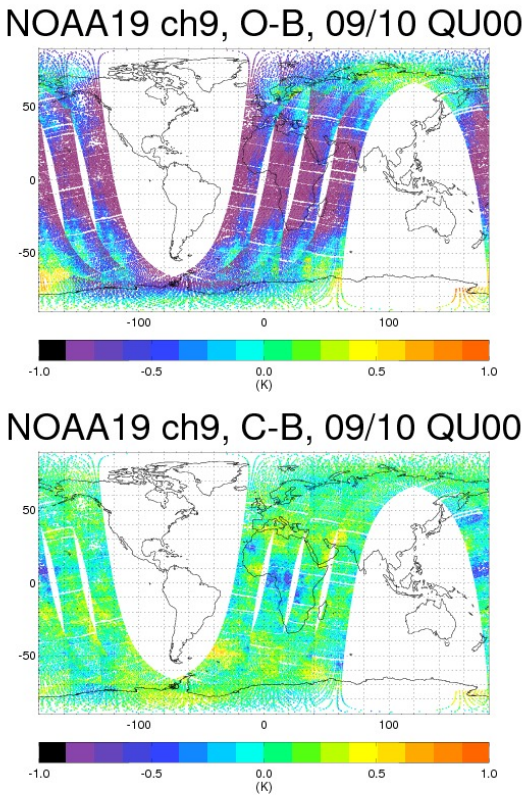

NOAA19 ch10, O-B, 09/10 QU00

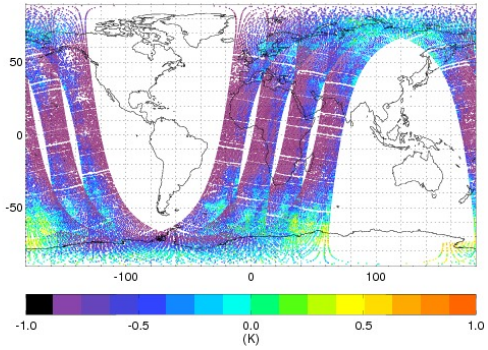

NOAA19 ch10, C-B, 09/10 QU00

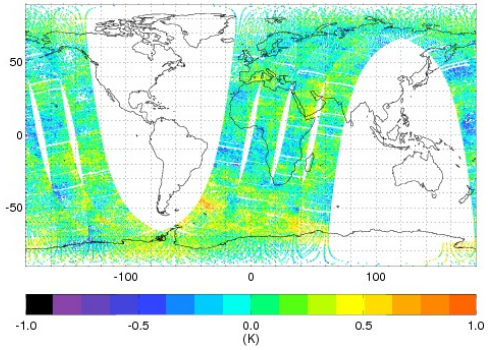

NOAA19 ch11, O-B, 09/10 QU00

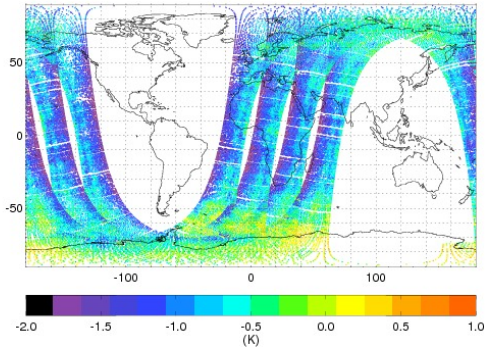

NOAA19 ch11, C-B, 09/10 QU00

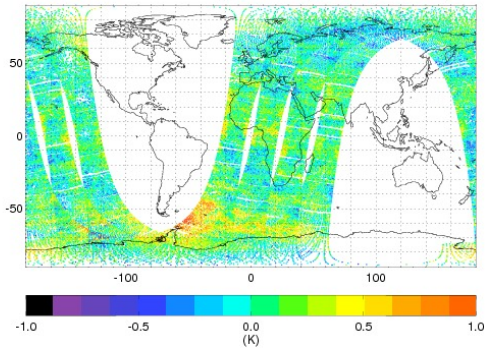

NOAA19 ch12, O-B, 09/10 QU00

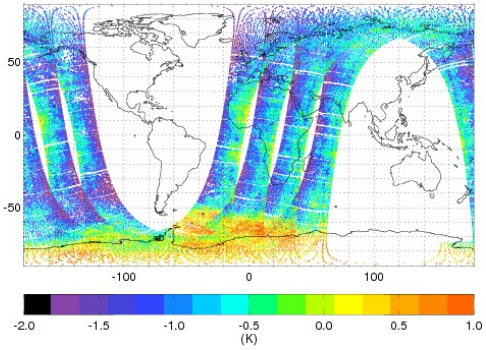

NOAA19 ch12, C-B, 09/10 QU00

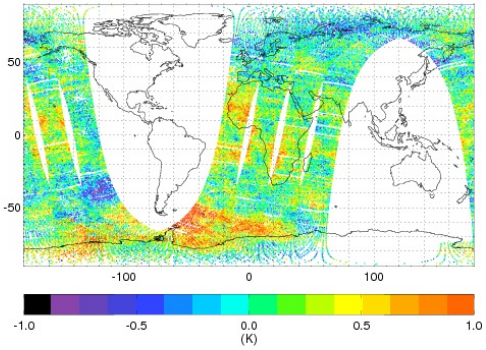

NOAA19 ch13, O-B, 09/10 QU00

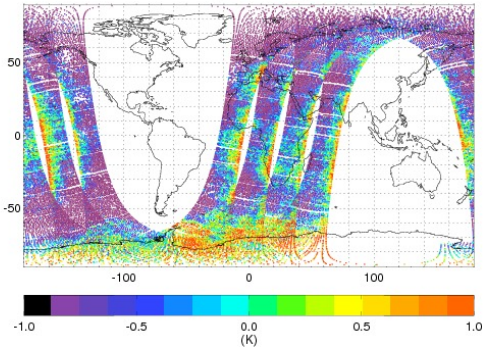

NOAA19 ch13, C-B, 09/10 QU00

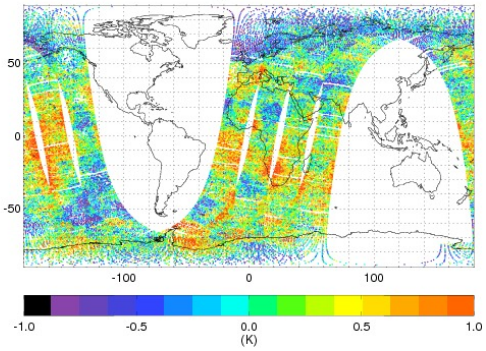

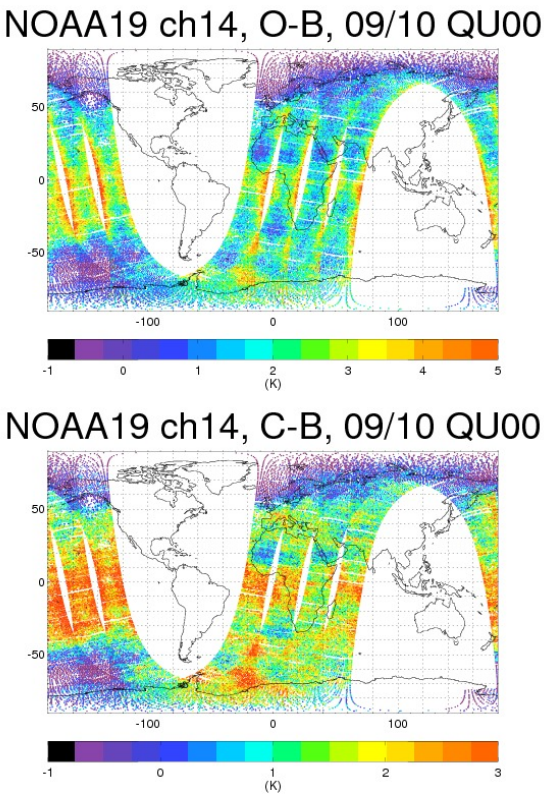

Figure 4: O-B (left) and C-B (right) for N19 AMSU channels 6-15 at 0Z on 30th July

Figure 5 shows the effect of the two thickness predictors in the static bias correction scheme on the variance of the innovations for ATMS, compared with the same plots for the AMSU instruments on NOAA-19 and Metop-A. The behaviour of the scheme is broadly comparable for ATMS and AMSU. Significant variance reductions are achieved using these predictors with either predictor capable of reducing the innovation variance significantly. For most channels there is significant benefit in using both predictors. Figure 5 shows that the sequential application of these predictors, with the 850-300 hPa predictor applied first, has the expected channel dependency: the 850-300 hPa predictor reduces the variance most effectively for the low peaking temperature sounding channels and the influence of the 200-50 hPa predictor becoming progressively stronger for the higher peaking channels.

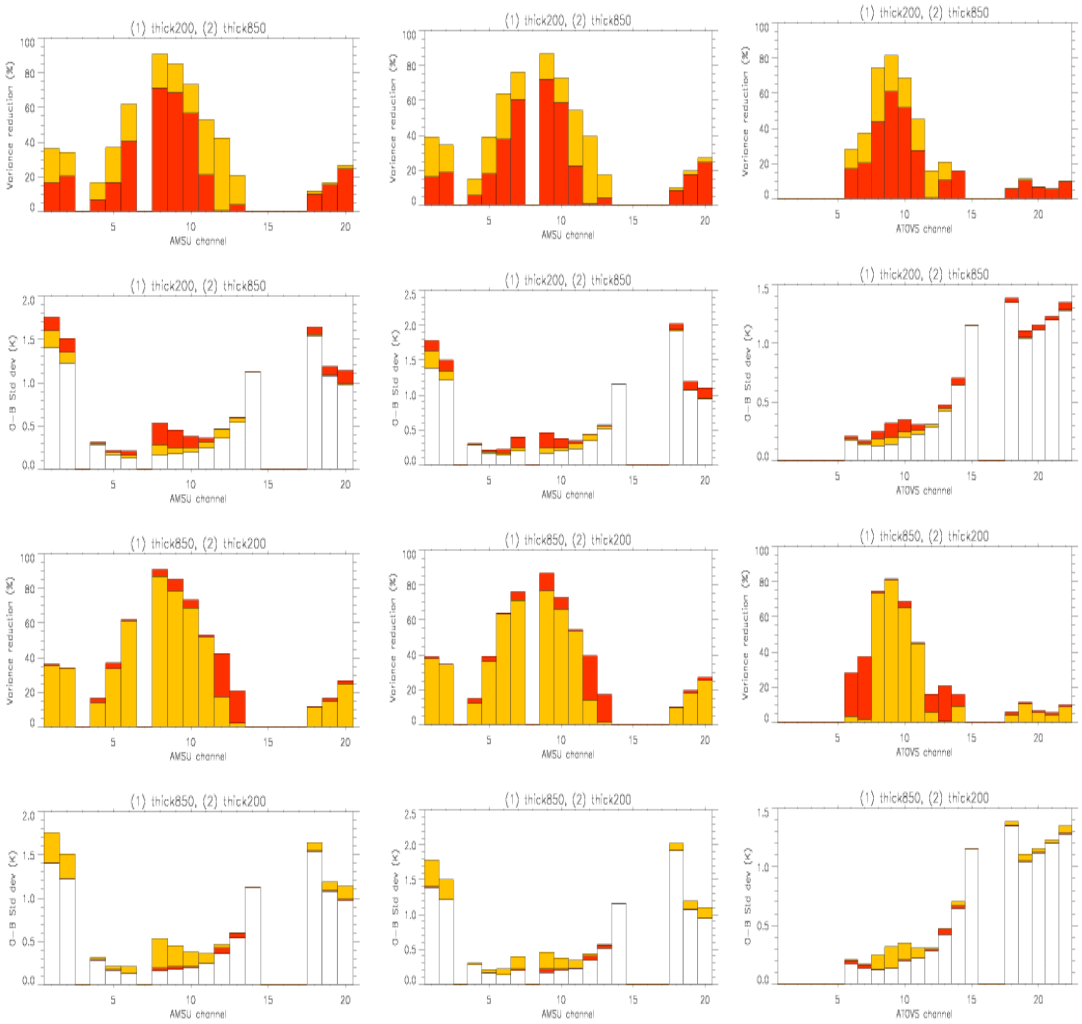

a b c

Figure 5: Effectiveness of the thickness bias predictors in reducing variance, for a) Metop-A, b) NOAA-19 and c) ATMS. Top 2 rows: 200-50hPa thickness predictor applied first; bottom 2 rows: 850-300hPa thickness predictor applied first

For all channels, an irregular striping pattern is visible in the maps of C-B. This is illustrated clearly in Figure 6 in the C-B plot for channel 14 in the equatorial Pacific but is evident throughout the orbit. The amplitude of the stripes is several tenths of a Kelvin. As background errors are generally below 100 mK for the tropospheric and lower stratospheric temperature sounding channels this effect is potentially a significant concern and is discussed further in Section 2.6.

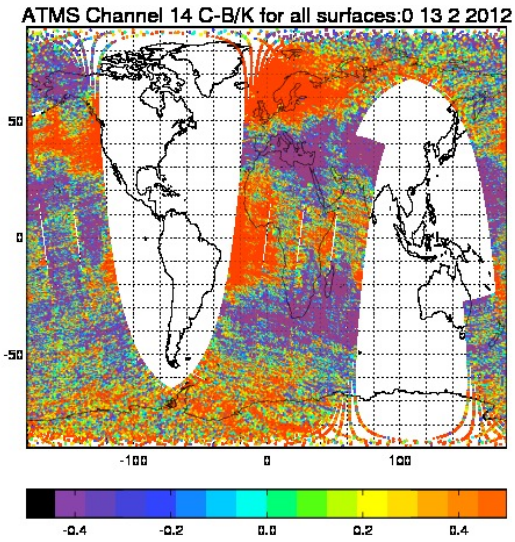

Figure 6: C-B plot showing striping effect on ATMS channel 14.

2.4 O-B comparisons

Means and RMS values of corrected minus background (C-B) and observed minus background (O-B) brightness temperature were computed each 6 hour cycle during the period 18th January to 18th February 2012. Figure 7 shows the C-B statistics plotted as a time series for ATMS channels 6-15 and 18, 20 and 22 and the corresponding channels on the three AMSU on Metop-A, NOAA-18 and NOAA-19.

The residual global mean biases in the ATMS corrected innovations are, in most cases, larger than for the equivalent AMSU channels, although for most of the key tropospheric channels the magnitude of the residual bias is less than 40 mK. In many cases the ATMS mean biases are twice the magnitude of the AMSU equivalents. This may reflect the limited time period (2 weeks) used to generate the bias corrections for ATMS. It is not clear whether this will have a significant impact on the assimilation of the ATMS as the analysis and forecast accuracy will be more strongly affected by the local form and amplitude of the biases. We expect improvements when the bias corrections are generated over a longer period.

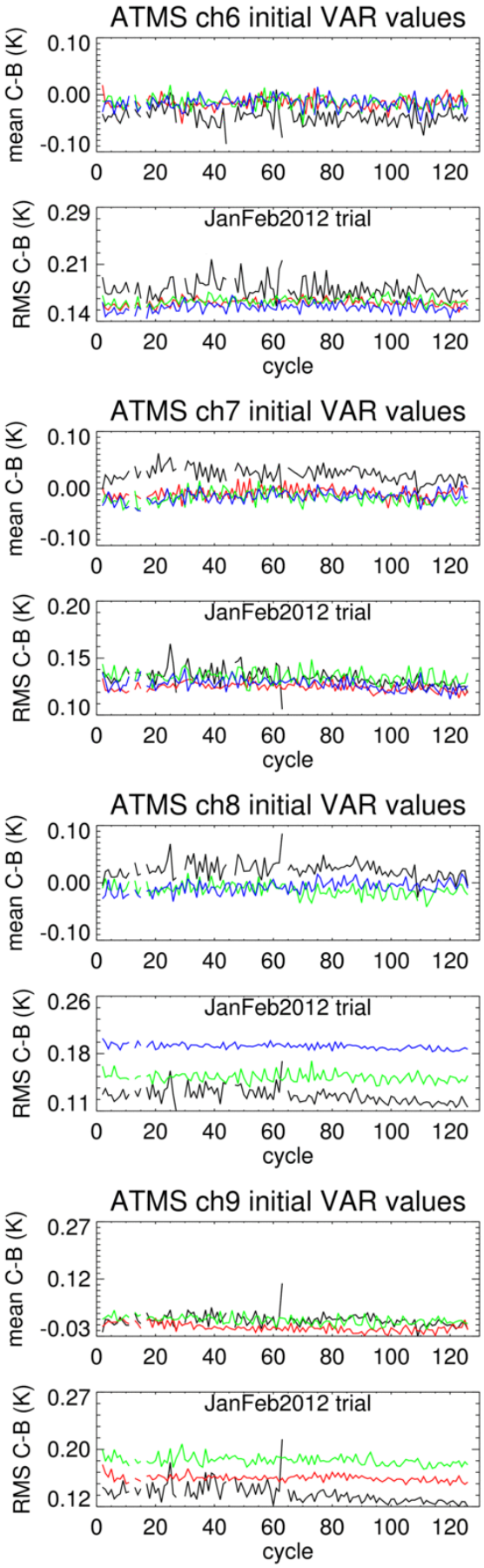

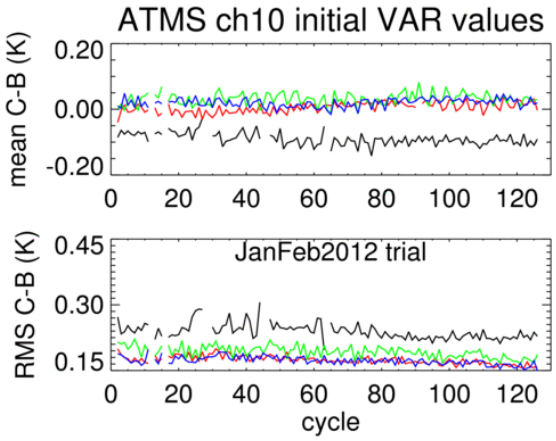

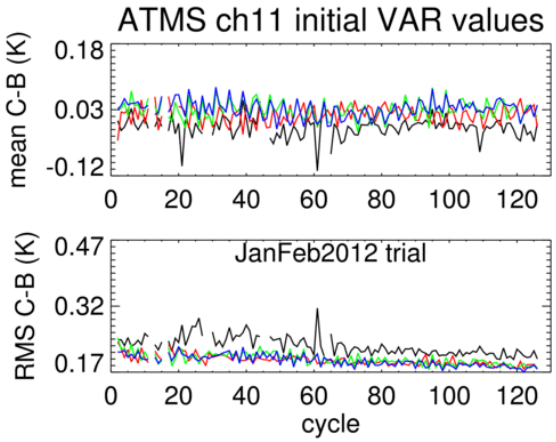

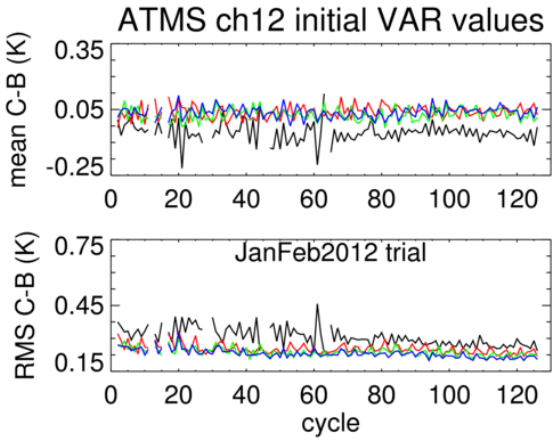

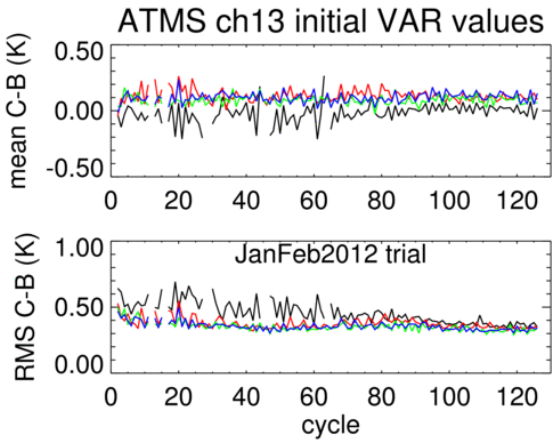

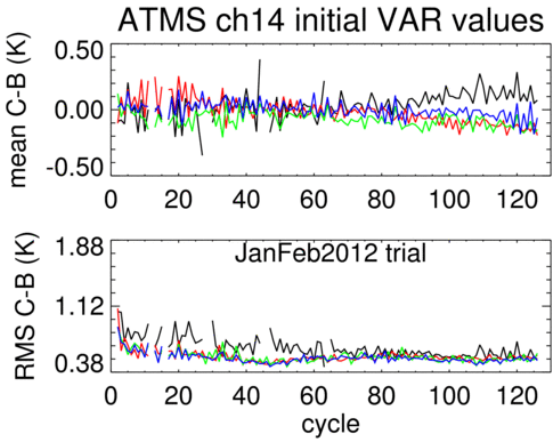

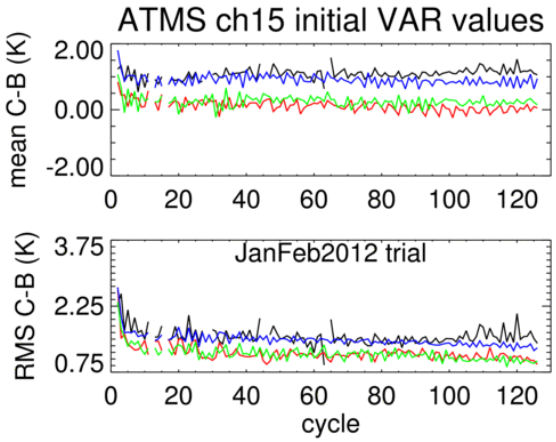

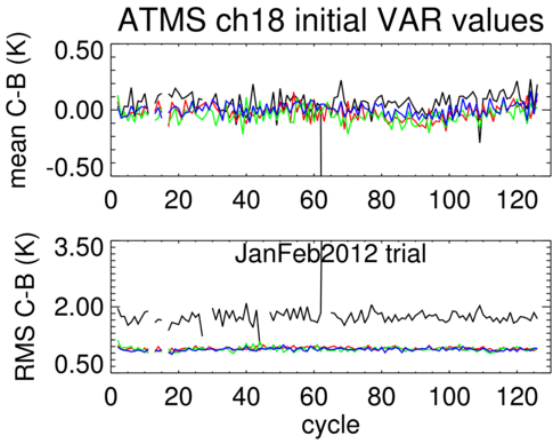

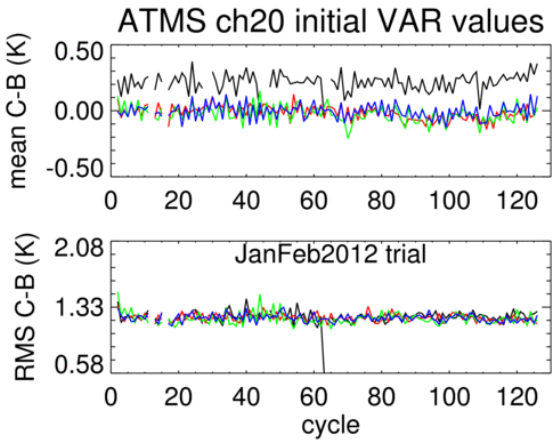

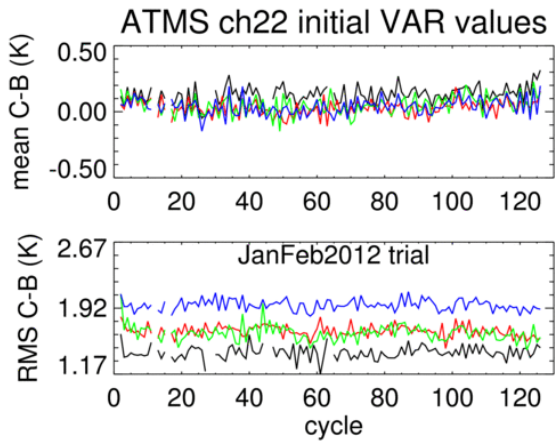

Figure 7: Time series of mean and standard deviation of C-B for ATMS and AMSU for the inflated R trial from 18 Jan to 18 Feb 2012. Black line=ATMS, red line=Metop, green line=NOAA-18, blue line=NOAA-19

For all temperature sounding channels the standard deviations of the corrected innovations (C-B) are significantly larger for the first half of the trial period. This pattern is most evident in the ATMS channels with weighting function peaks in the troposphere and lower stratosphere (6-10) and is much less pronounced in the AMSU equivalent channels. The same pattern is evident in the higher peaking temperature sounding channels (11-15) for both AMSU and ATMS although it is, again, less pronounced for AMSU. Figure 8 shows the number of ATMS observations going in to 4D-Var over the course of the trial and there is a marked increase in number processed with fewer data dropouts and less variablility for the second half of the trial, from run 80 onwards.

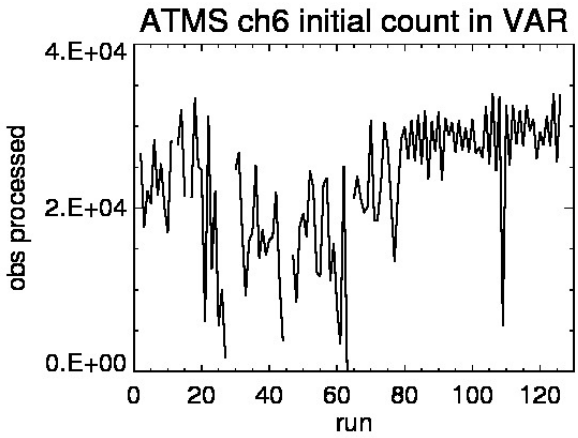

Figure 8: Time series of number of ATMS observations accepted for processing for the inflated R trial.

The apparent variation in data quality through the trial period is discussed again in Section 3, where it is shown that forecast verification of the latter half of the period gives more positive results than the results over the period as a whole, although significance can only be attached to verification results for shorter range forecasts (< T+72 hours).

For the humidity sounding channels Figure 7 shows no clear pattern in the relative performance of ATMS versus the equivalent AMSU channels: for example the standard deviations of corrected innovations are higher for ATMS in Channel 18 (183±7.0 GHz) compared to AMSU (1.8 K compared to 1.0 K) whereas for channel 22 (183±1.0 GHz)

the standard deviations of the corrected innovations are smaller for ATMS (1.4 K compared to 1.8 K for AMSU)

There is also a spike in most channels (in particular see channels 9, 11, 18, 20, Figure 7) at cycle 63, which may indicate some poor data for that time period.

Figure 9 shows the histograms of uncorrected and corrected innovations for AMSU channels 1-20 together with those for the equivalent ATMS channels. The distributions are broadly similar, with the noticeable exception of ATMS channels 11-14 which show a warm tail. Figure 9 illustrates how well the bias corrections are working, the curves become more Gaussian after bias correction is applied and move to be more closely centred on zero. The AMSU bias correction process is obviously working better in some channels (e.g. ATMS channel 10, AMSU channel 9), though in others (e.g. ATMS channel 9) the ATMS corrected histogram is more closely centred on zero and more Gaussian in shape showing that the ATMS bias correction is working exceptionally well and much better than the AMSU bias correction. The plots in Figure 9 also demonstrate the quality of the uncorrected data. In some cases (e.g. ATMS channels 6 and 7) the green curve (AMSU uncorrected) is significantly farther from zero than the red curve (ATMS uncorrected).

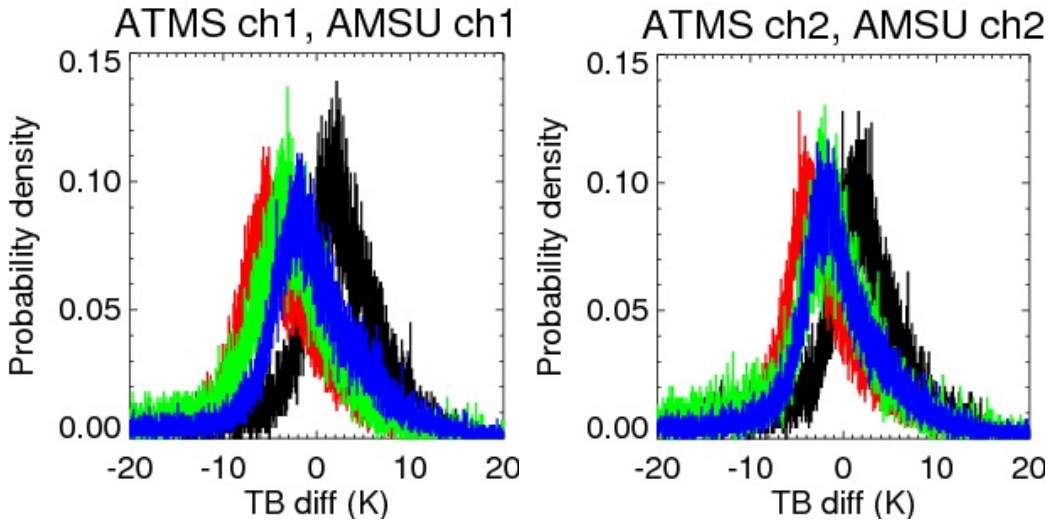

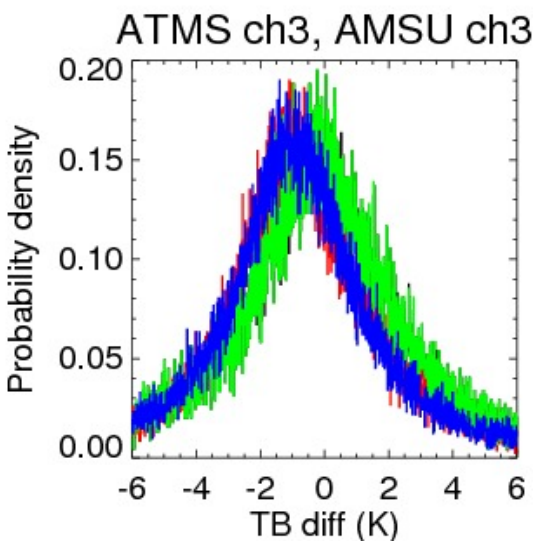

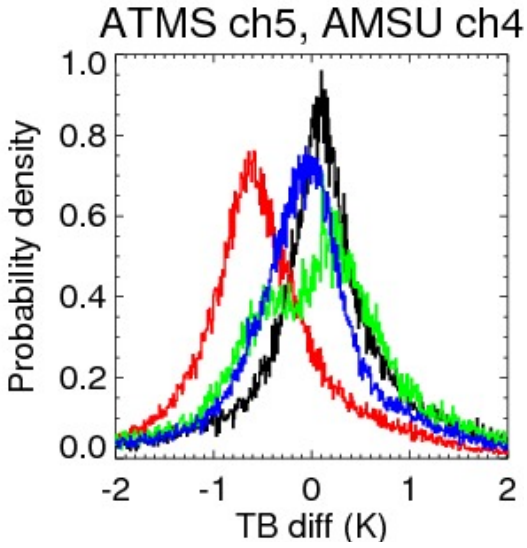

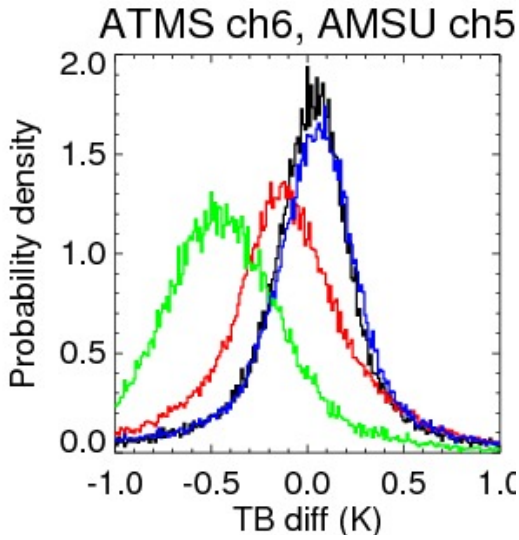

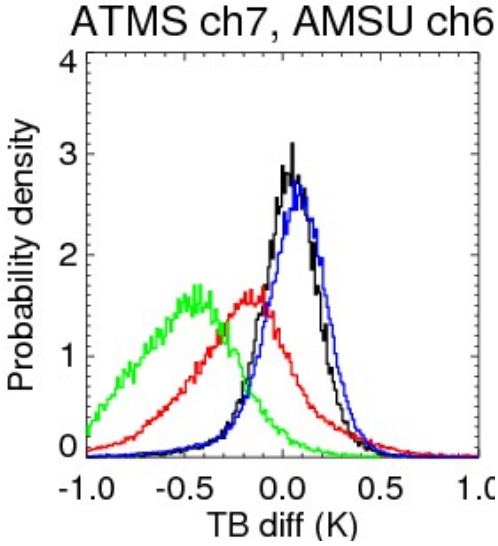

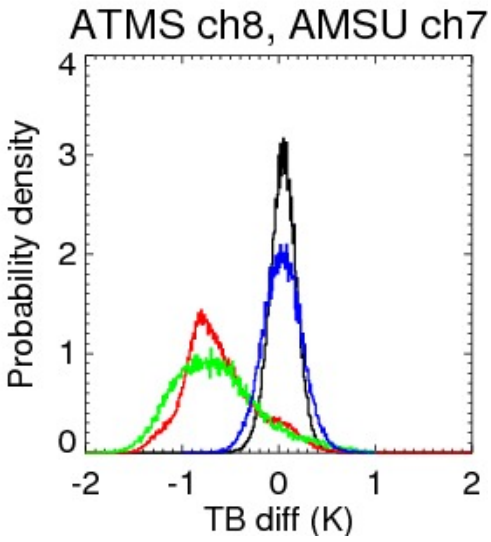

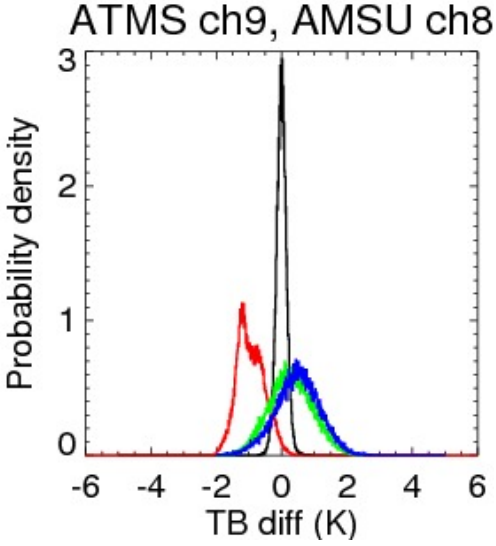

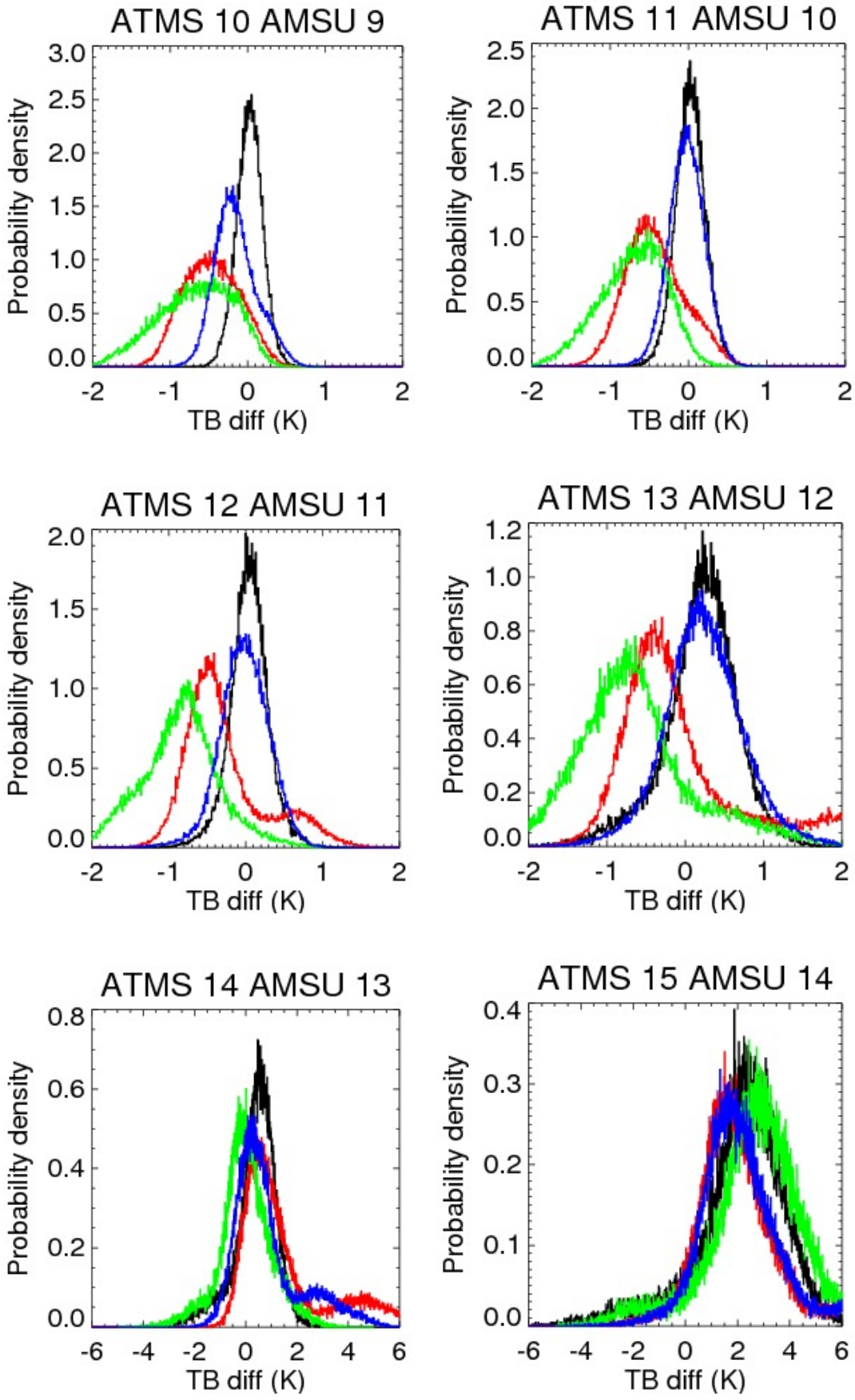

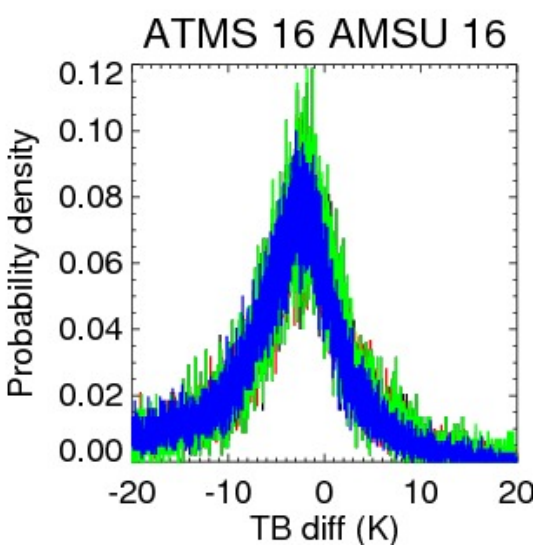

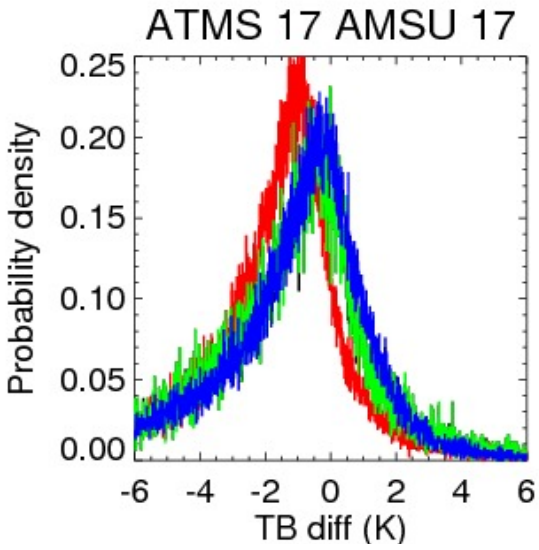

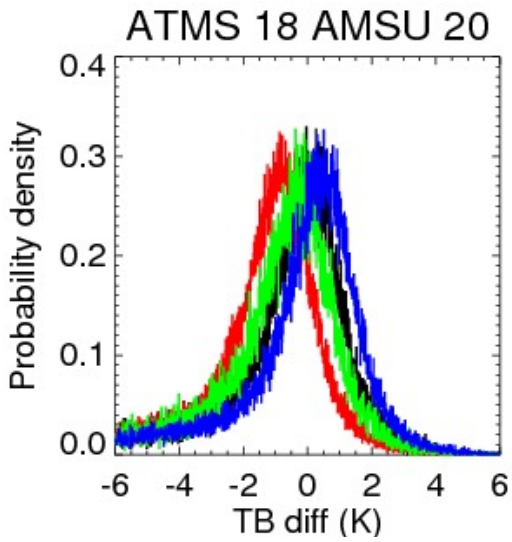

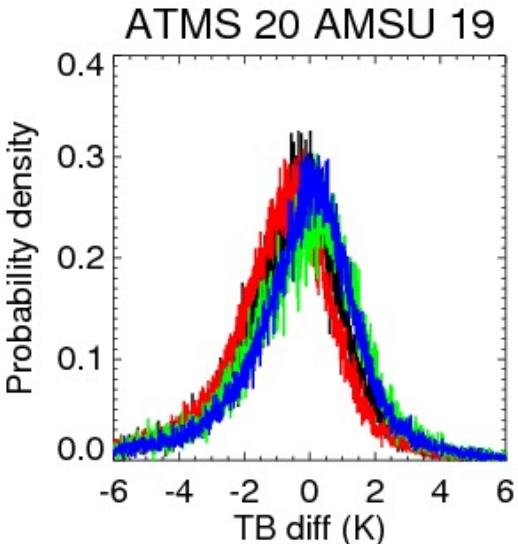

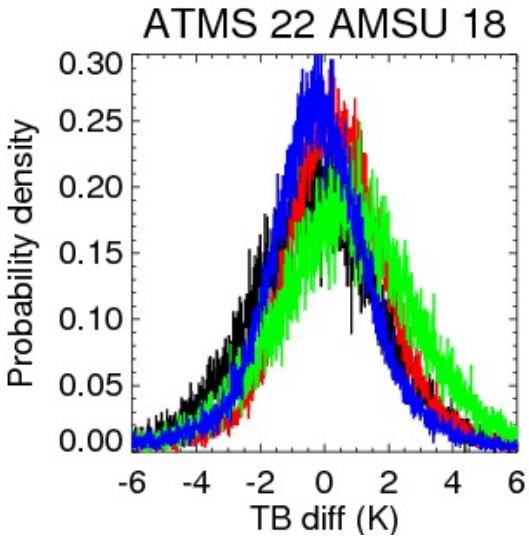

Figure 9: Normalisted pdfs of O-B and C-B for ATMS and AMSU. In most of the plots green to black shows the AMSU uncorrected to corrected change and red to blue shows the same for ATMS. For channels 8 and 9 the colour scheme is green to blue for AMSU and red to black for ATMS.

Figure 10 gives a summary of the global O-B and C-B values, grouped as temperature sounding channels (Figure 10a), humidity sounding channels (Figure 10b) or window channels (Figure 10c) compared to equivalent AMSU channels.

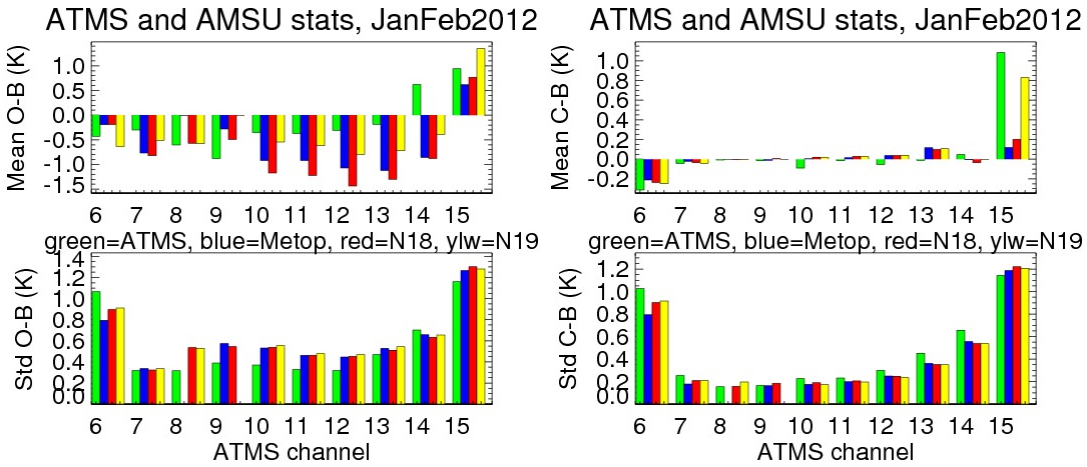

a

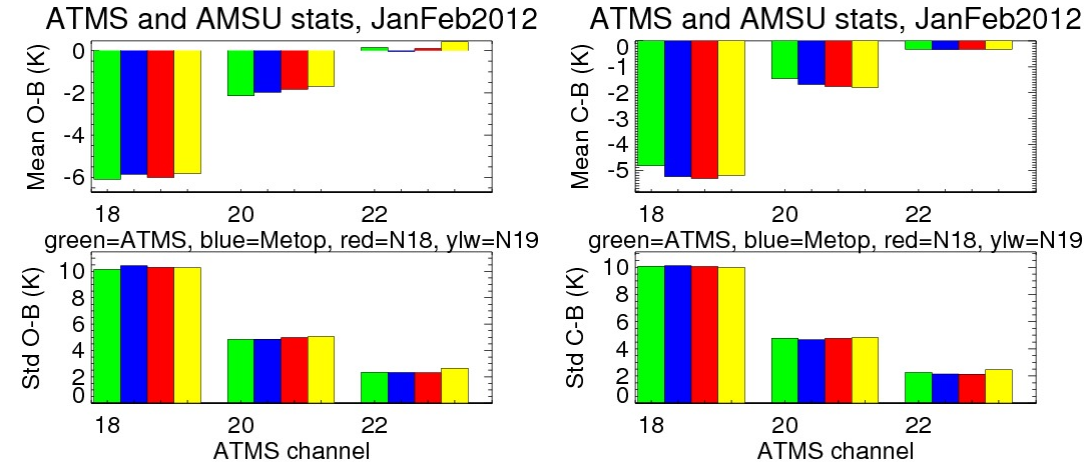

b

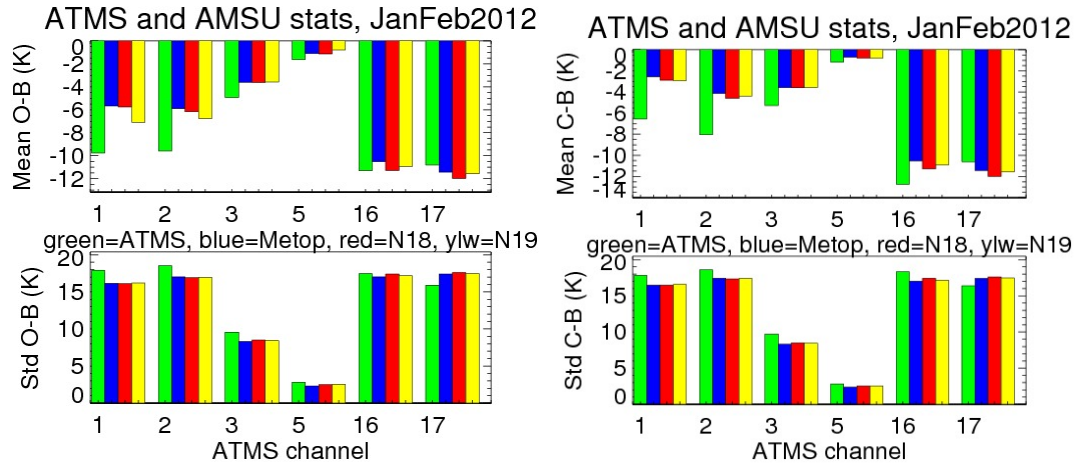

c

Figure 10: standard deviation and mean of O-B and C-B for ATMS, and 3 AMSUs. a) temperature sounding channels, b) moisture sounding channels, c) surface viewing channels.

For the temperature sounding channels Figure 10a shows that the mean O-B are of a similar magnitude for ATMS and AMSU. Indeed for ATMS channels 10-13 the mean biases for ATMS are smaller than for the equivalent AMSU channels. The standard deviations of O-B for ATMS channels 7-13 are smaller than the equivalent AMSU channels. Generally the bias correction is effective in reducing the mean C-B to close to zero for the temperature sounding channels, however the standard deviation for channels 10-14 remains larger for ATMS compared to AMSU equivalents.

Figure 10b shows that for the humidity sounding channels the mean and standard deviations of the innovations are similar for ATMS and AMSU. For the surface viewing channels (Figure 10c) the statistics are broadly similar.

These statistics can also be split up into latitude bands. Figure 11 shows the same plots as Figure 10, except for the latitude range -20º to -70º. All other latitude bands were broadly similar to the global results, but the range -20º to -70º has some differences. Notably significantly smaller mean values for the surface viewing channels (Figures 10c and 11c), with a different sign for channel 1 and 2 mean C-B. And significantly smaller O-B and C-B mean values for the moisture sounding channels (Figures 10b and 11b). The temperature sounding channels show higher mean O-B in the southern latitude band than for the global case, as would be expected given the warm bias in the temperature sounding channels already noted in Section 2.3, with standard deviations significantly smaller.

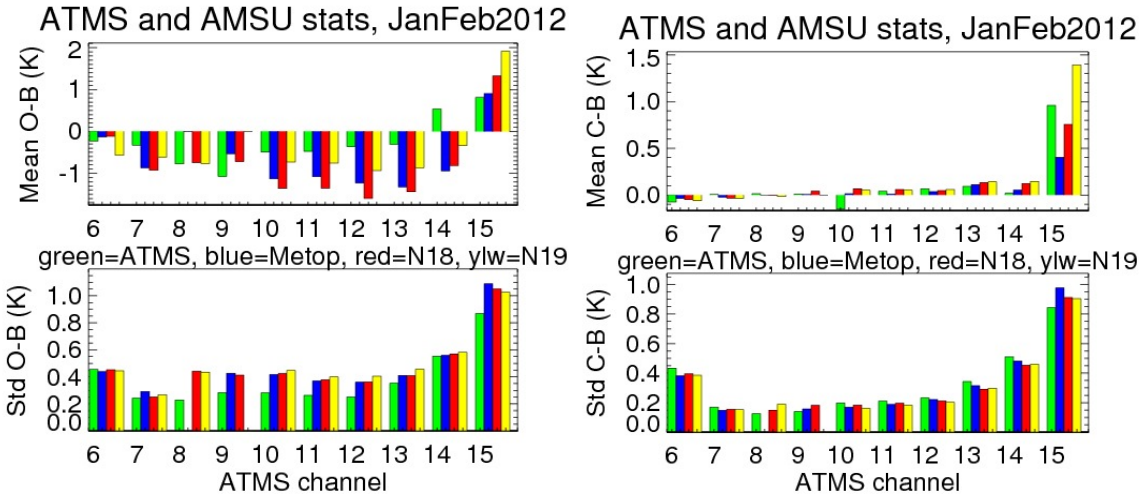

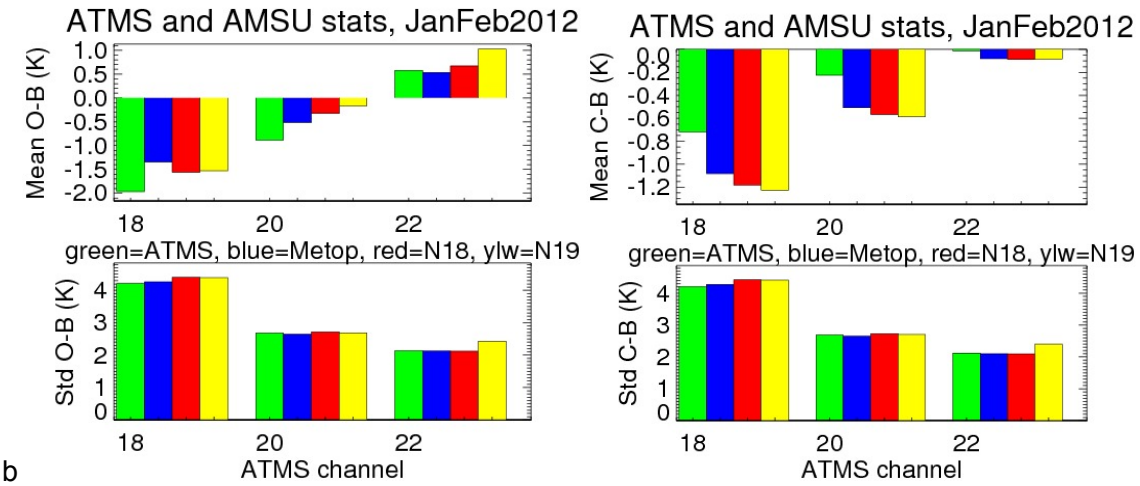

b

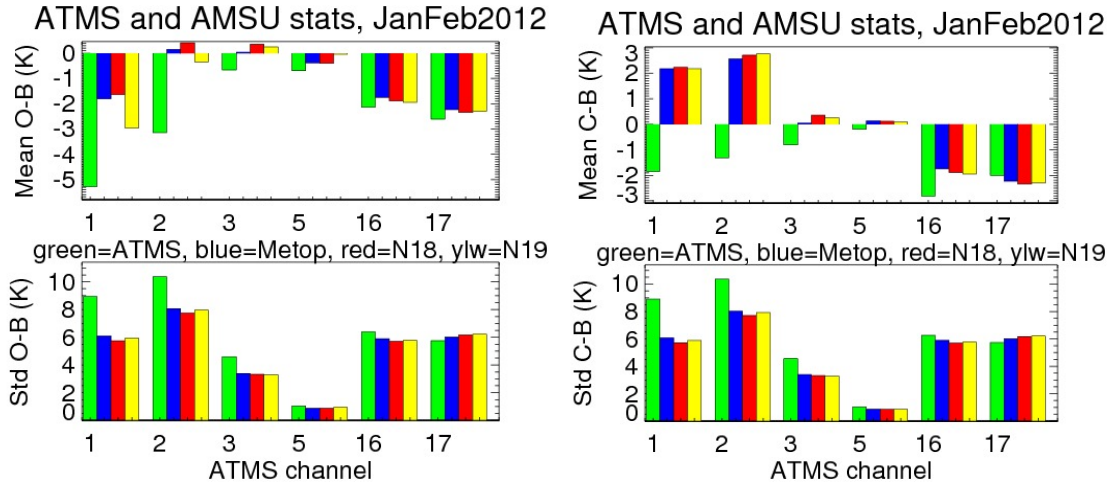

c

Figure 11: Statistics for Jan/Feb 2012 for latitude band -70º to -20º. a) temperature sounding channels, b) moisture sounding channels, c) surface viewing channels.

A time series of ATMS O-B and C-B for channels 7 and 8 is shown in Figure 12. This is for the period 1st July to 1st August 2012. Figure 13 shows the number of observations processed for this period. Figure 12 demonstrates again that bias correction is working effectively, shifting the mean (blue line) towards zero, other channels, not shown, exhibit similar patterns. Figure 13 demonstrates that the data is relatively stable over the summer period after near real time data began flowing on 27th June 2012, the expected number of observations are being processed, usually more than 80000 in each cycle, although this can be quite variable. The change in variability of number of observations processed around the 5th of July corresponds to a shift in the timing of the monitoring to allow more observations to arrive. Figure 14 shows the delay in arrival of global ATMS data to the Met Office on 25 September 2012.

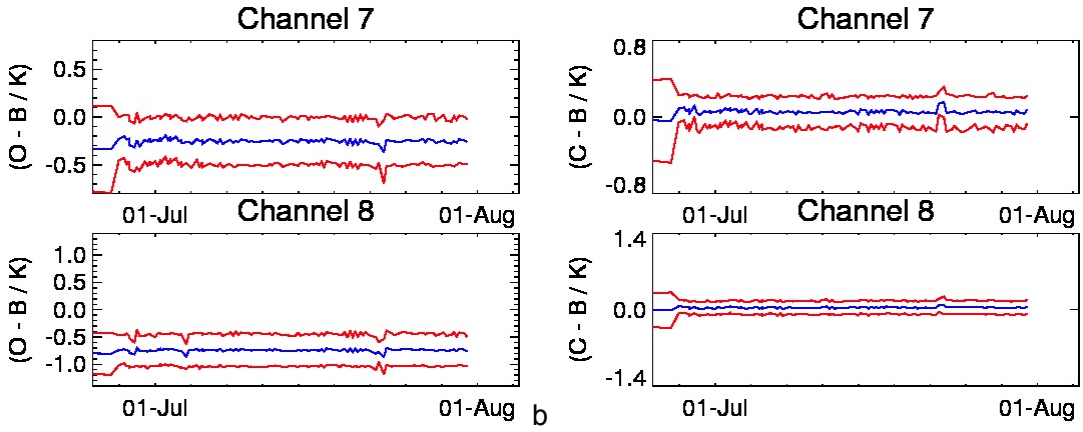

Figure 12: ATMS channels 7 and 8 timeseries of mean (blue line) +/- 1standard deviation.a) uncorrected, b) corrected

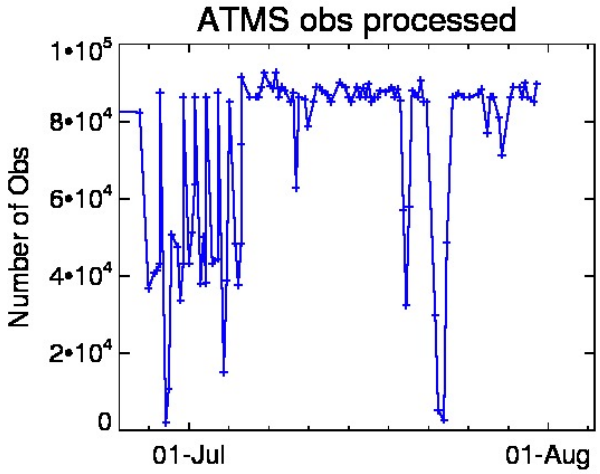

Figure13: Number of ATMS observations processed in OPS.

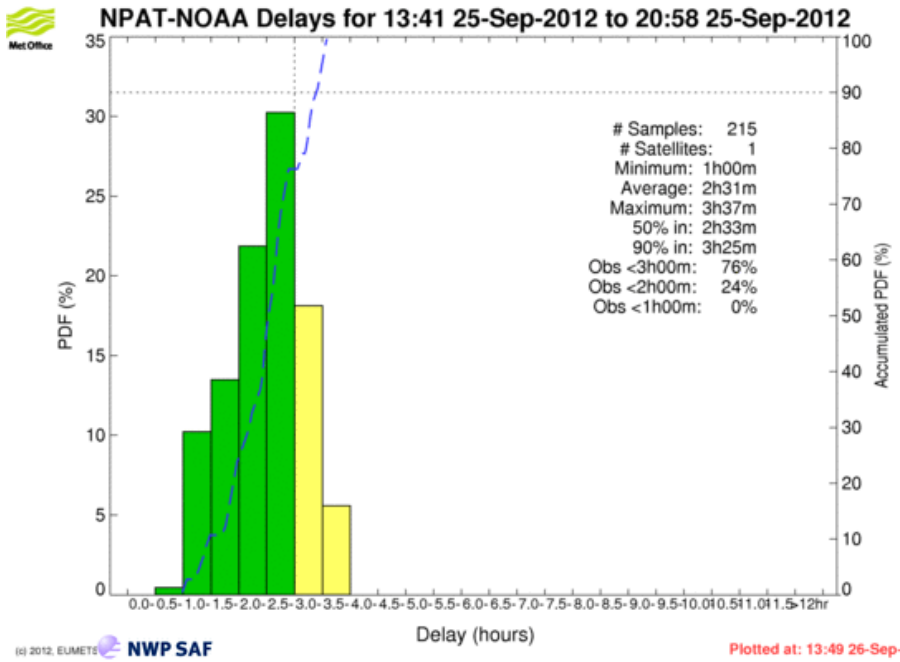

Figure 14: Delay in arrival of ATMS data from the global data stream. The vertical dotted line shows the operational cut-off time of 3 hours, data arriving before this time (green

bars) will be included in the main run of the forecast model, data arriving after this (yellow bars) will be included in the update run (D. Offilier pers. comm.).

2.5 Radiometric Performance

This section gives a brief discussion of the ATMS data quality, in terms of the radiometric performance on-orbit, by comparison with AMSU data from Metop-A, NOAA-18 and NOAA-19. The effective NEΔT for the ATMS data is improved through the AAPP re-mapping. For the AAPP configuration used in these experiments the theoretical noise reduction factors are 0.72, 0.30 and 0.23 for channels 1-2, 3-15 and 16-22 respectively. These factors assume the noise is random; the contribution of non-random noise (i.e. noise that shows correlations between adjacent samples) will tend to increase the scan-to-scan variability and is excluded.

ATMS effective NEΔT for the remapped ATMS data from AAPP are shown in Table 2 for 03/07/12, alongside Metop-A and NOAA19 AMSU/MHS warm load effective NEΔT data. The values given for AMSU are those for Feb 2012. The ATMS NEΔT values are as good as and generally better than the equivalent Metop and NOAA-19 values. Figure 15b includes the values for standard deviation of C-B for ATMS. It can be seen from Table 2 and Figure15 that the std(C-B) values are markedly higher than the warm effective NEΔT. The source of this increased noise is likely threefold: (i) the striping effect mentioned in Section 2.3 and discussed further in Section 2.6, (ii) errors in the model background and (iii) residual bias.

Table 2: Noise performance for ATMS and MetopA/NOAA19 AMSU/MHS.
MHS values are for MHS mapped to the resolution of AMSU (a factor 0.34 lower than the raw NEDT).

ATMS					MetopA NEDT /K at 280 K	NOAA 19 NEΔT / K
Channel	Warm NEDT (effective)	Cold NEDT (effective)	Pre-launch spec x reduction due to resampling	Std dev C-B		
1	0.16	0.06	0.36	17.82	0.18	0.17
2	0.19	0.07	0.43	18.59	0.22	0.16
3	0.09	0.04	0.21	9.72	0.34	0.21
4	0.06	0.03	0.15	5.97	-	-
5	0.06	0.03	0.15	2.81	0.14	0.13
6	0.07	0.03	0.15	1.02	0.18	0.15
7	0.06	0.03	0.15	0.25	0.14	0.13
8	0.06	0.03	0.15	0.15	-	0.22
9	0.07	0.04	0.15	0.16	0.18	0.67
10	0.10	0.05	0.23	0.23	0.18	0.16
11	0.14	0.07	0.30	0.23	0.23	0.22
12	0.15	0.07	0.30	0.30	0.27	0.23
13	0.23	0.12	0.45	0.45	0.37	0.34
14	0.31	0.16	0.66	0.66	0.52	0.49
15	0.51	0.27	1.08	1.14	0.84	0.78
16	0.04	0.03	0.07	18.31	0.10 / 0.07	0.12/0.07
17	0.06	0.05	0.14	16.38	0.12	0.13
18	0.06	0.05	0.18	10.08	0.18	1.19
19	0.06	0.05	0.18	7.15	-	-
20	0.08	0.07	0.18	4.79	0.14	0.22
21	0.09	0.07	0.18	3.00	-	-
22	0.12	0.09	0.23	2.25	0.12	0.11

a

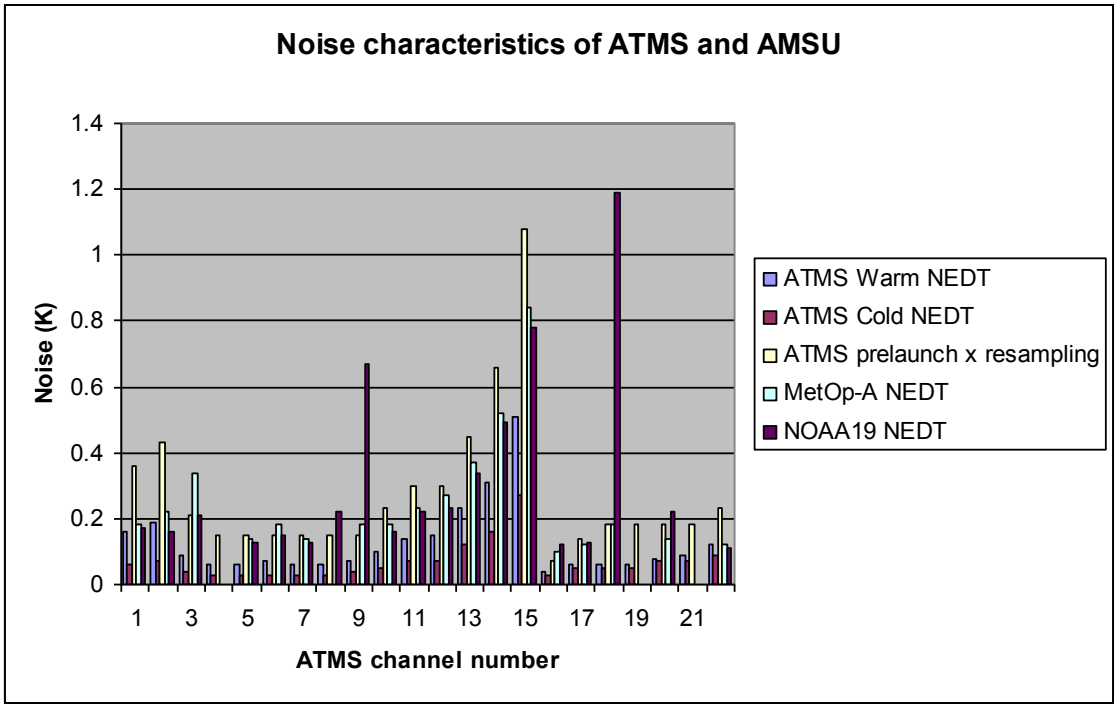

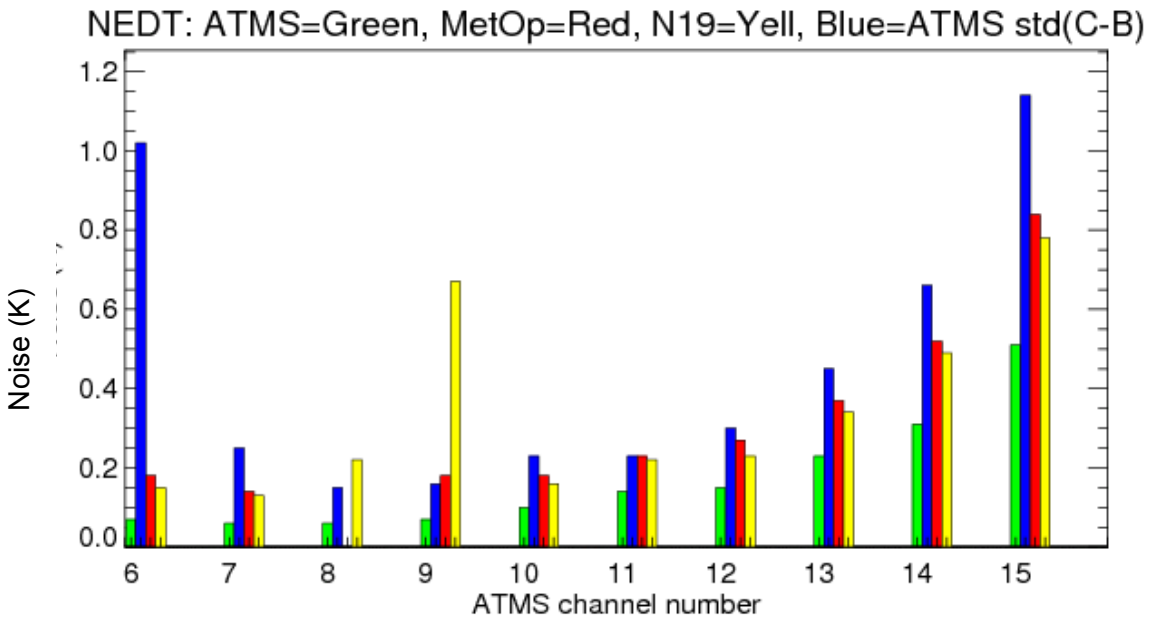

b

Figure 15: Noise characteristics of ATMS and AMSU: showing the data from Table 2. 15a: All ATMS channels, 15b: ATMS temperature sounding channels

2.6 Investigation into Striping

The striping effect mentioned in section 2.3 is present in all channels and most evident for channels 6-15. Its amplitude is sufficiently large (several tenths of a Kelvin) potentially to affect adversely the impact of the ATMS data on the analysis. The effect is illustrated in Figure 16, which shows the C-B values for channel 8 at 0Z on the 15th July 2012.

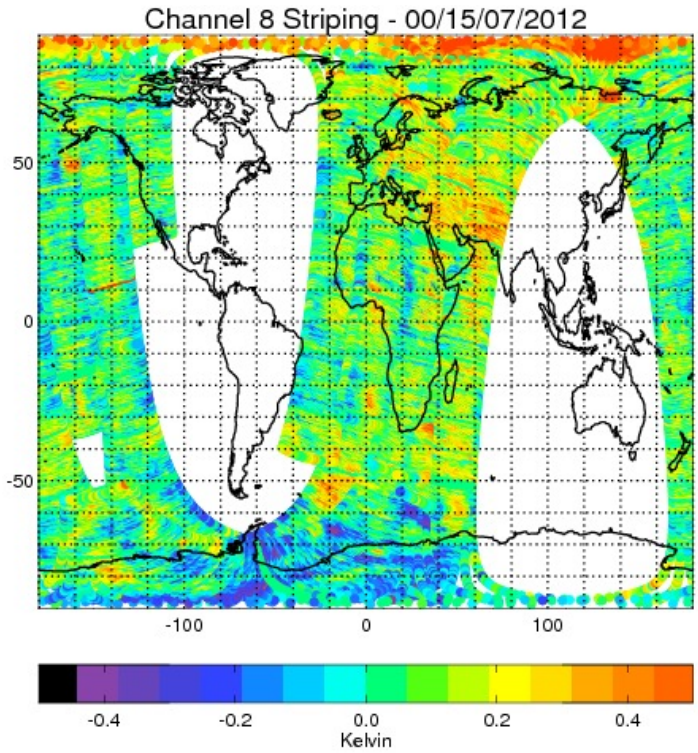

Figure 16: C-B values for ATMS channel 8 on 15/02/12 clearly showing the striping effect.

Investigation into the striping signal in the raw instrument counts from the data has been undertaken. This investigation aimed to

1. Demonstrate a method to quantify the additional variability associated with striping, using observations alone.
2. Ascertain if the striping is visible in the raw counts, as well as the calibrated brightness temperatures (BT).
3. Establish whether increasing the averaging time for the calibration views (i.e. using more scans) would reduce the effect of the striping.

2.6.1 Locally received sample data

Direct readout data over Exeter was used for the period 01:43 to 01:54 on 13th August 2012. The University of Wisconsin Community Satellite Processing Package (CSPP)[iii] was modified to permit the generation of verified raw data records (RDRs), in addition to the usual temperature data records (TDRs) and Sensor Data Records (SDRs). The verified RDRs contain the raw counts.

The calibrated antenna temperatures were obtained from the TDRs using AAPP. (Note that the brightness temperatures in the SDRs still have incorrect antenna pattern correction in CSPP, so are not used). Coverage is shown in

Figure 17.

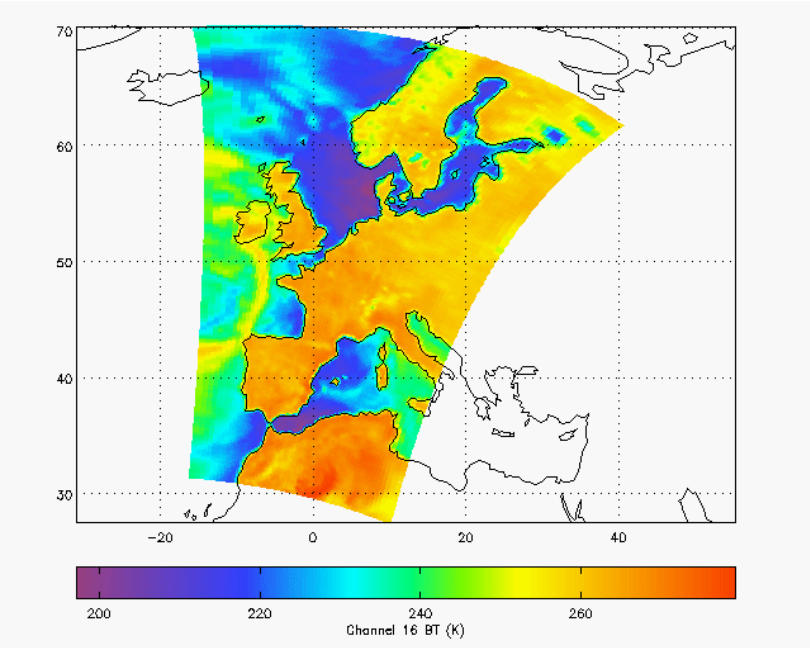

Figure 17: ATMS channel 16, 20120813 01:43 to 01:54

The SDRs contain an internal estimate of NEΔT: 1 warm NEΔT and 1 cold NEΔT per scan line. This is defined as the standard deviation of the four cold/warm calibration view readings divided by the gain (to convert from counts to Kelvin). This estimate of NEΔT does not account for any noise sources that have a time scale longer than 4 times the integration time.

2.6.2. Analysis of striping in brightness temperatures

To show the noise clearly it is necessary to remove as much of the atmospheric signal as possible. An effective way of doing this is to look at the difference between the measured brightness temperature (BT) (or raw counts) and BT (or counts) that are obtained by passing the field through a spatial filter that removes fine structure. For this study the fast fourier transform method described in NWP SAF (2011a) was used, with a beam width of 5.2°, i.e. degrading the sounding channels 3-15 to the resolution of channels 1-2. 3 samples at each edge of the scan were also discarded as these are contaminated by edge effects, leaving 90 samples remaining.

For channels 7-15, which are not sensitive to the surface, the resulting signal is dominated by instrument noise. The example of this in Figure 18 shows evidence of horizontal stripes in channel 9 brightness temperature differences.

Figure 18: Channel 9 BT difference (unprojected): unfiltered minus filtered brightness temperatures at 5.2º resolution. Scale is black to white: -1.0 K to +0.9 K.

To quantify the difference between the along-scan variability and the along-track variability a 90×90 region was selected and averaged separately in each direction, the resulting standard deviations were then calculated.

The results are shown in Figure 19 and Figure 20. For channels 7-13 the along-track variabilities (left hand plots) are a factor 2-3 larger than the cross-track variabilities (right hand plots). Note also that some inter-channel correlations are apparent – e.g. the positive spike at scan 36 in channels 7-9 and the negative spike at line 81 for all channels.

Note that in ATMS, channels 3-15 all share the same feedhorn, local oscillator (LO) and receiver front end – unlike AMSU-A, which has a separate LO/mixer for each of channels 3-8, with a shared LO/mixer for channels 9-14.

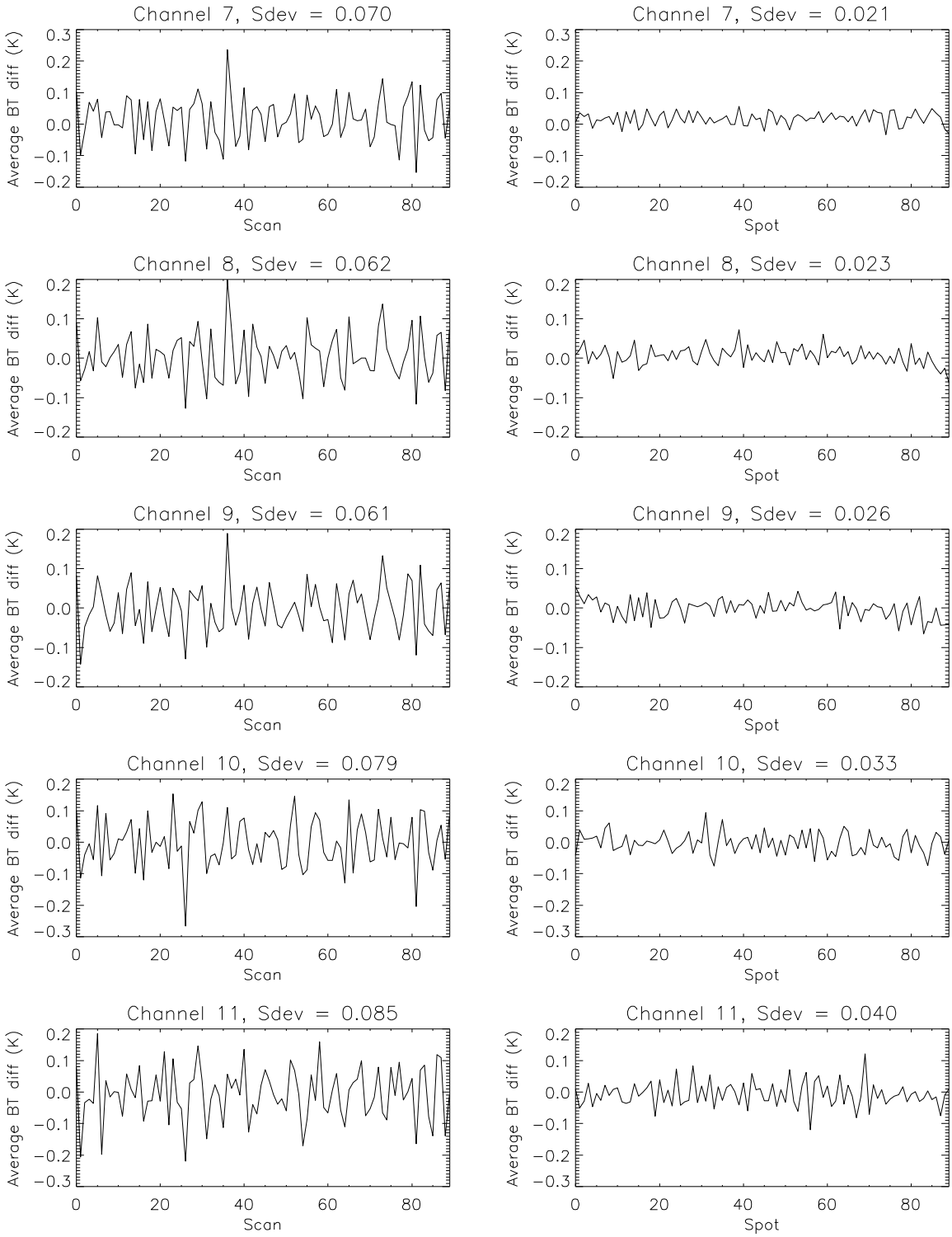

Figure 19: Along-track (left) and cross-track (right) brightness temperature differences for channels 7-11

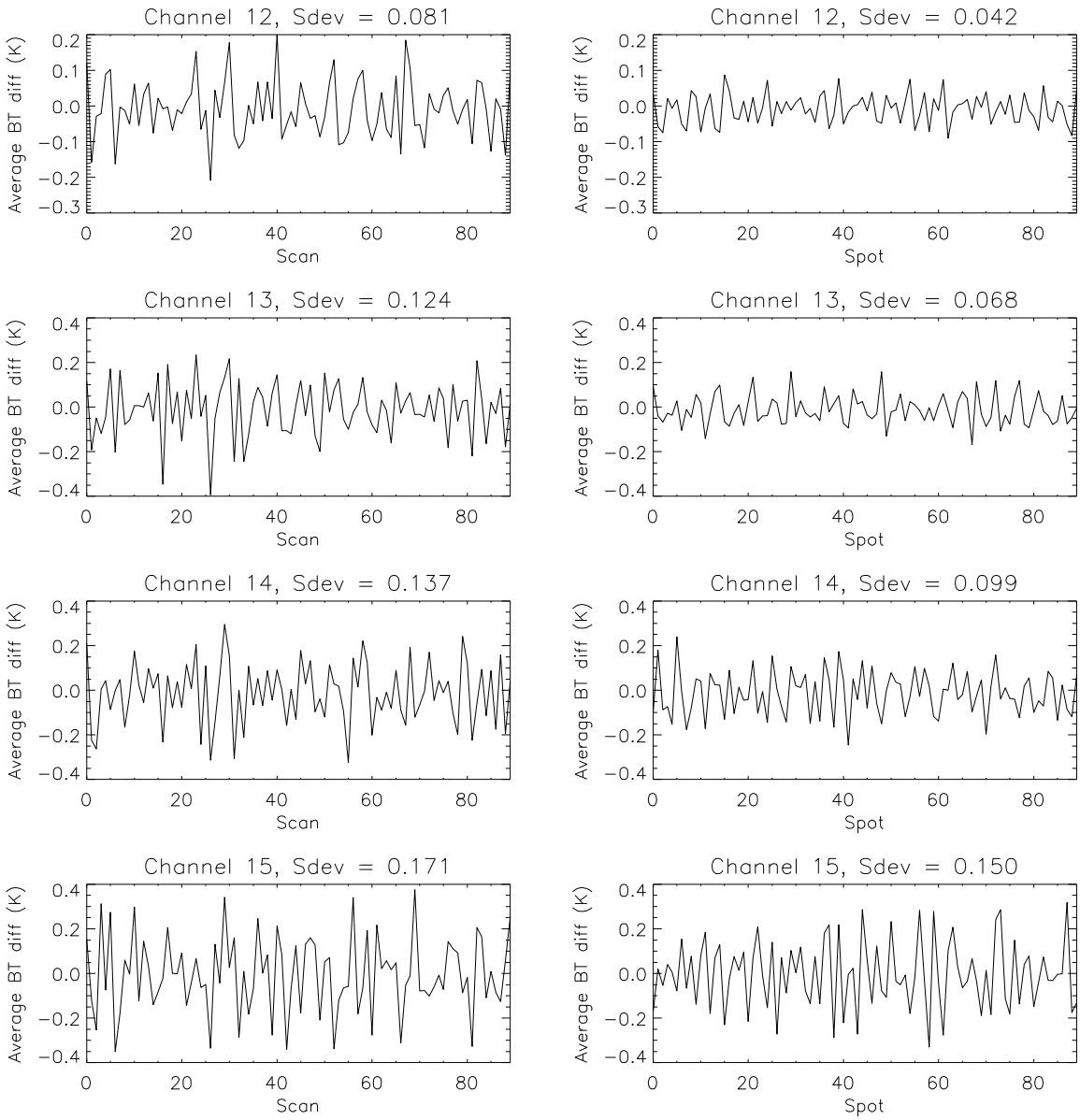

Figure 20; Along-track (left) and cross-track (right) brightness temperature differences for channels 8-15

It is useful at this point to compare the standard deviation of the BT difference field with the mean of the NEΔT values provided in the SDR file. See Table 3.

Table 3: NEΔT values compared with standard deviation of BT difference field. The "weighted NEΔT" is linearly interpolated from the warm and cold view NEΔTs, assuming the warm view is at 280K and the cold view is at 3K. The "local NEΔT" is the mean of the standard deviations of groups of 4 neighbouring pixels.

Channel	Mean BT (K)	Warm NEΔT (K)	Cold NEΔT (K)	Weighted NEΔT (K)	Local NEΔT (K)	Std dev of difference field (K)
7	236.8	0.21	0.11	0.20	0.20	0.23
8	227.0	0.21	0.11	0.19	0.19	0.22
9	221.0	0.24	0.13	0.22	0.22	0.24
10	219.2	0.35	0.18	0.31	0.30	0.34
11	222.3	0.50	0.24	0.45	0.41	0.45
12	228.1	0.50	0.26	0.45	0.44	0.48
13	235.9	0.77	0.39	0.71	0.67	0.73
14	245.9	1.01	0.54	0.95	0.97	1.04
15	254.4	1.69	0.91	1.62	1.61	1.70

The "local NEΔT" in Table 3 is computed in a similar way to the warm and cold NEΔT – from groups of 4 neighbouring pixels. The local NEΔT is in reasonably good agreement with the "weighted NEΔT" which originates from the calibration views.

The overall standard deviation of the difference field for this unfiltered data is in the range 0-15% larger than the weighted and local NEΔT values. Note that this is for data that has not been spatially filtered. The impact of the striping on the remapped data used in assimilation is discussed in Section 2.6.6.

2.6.3 Analysis of striping in raw counts

The analysis of the previous section was repeated using raw counts instead of brightness temperatures. The results, shown in 21 and 22, are very similar, leading to the following conclusions:

- The striping is an inherent property of the measured earth counts and is not significantly affected by the operational calibration algorithm.
- Increasing the calibration view averaging is unlikely to help, but this will be investigated further in subsequent sections.

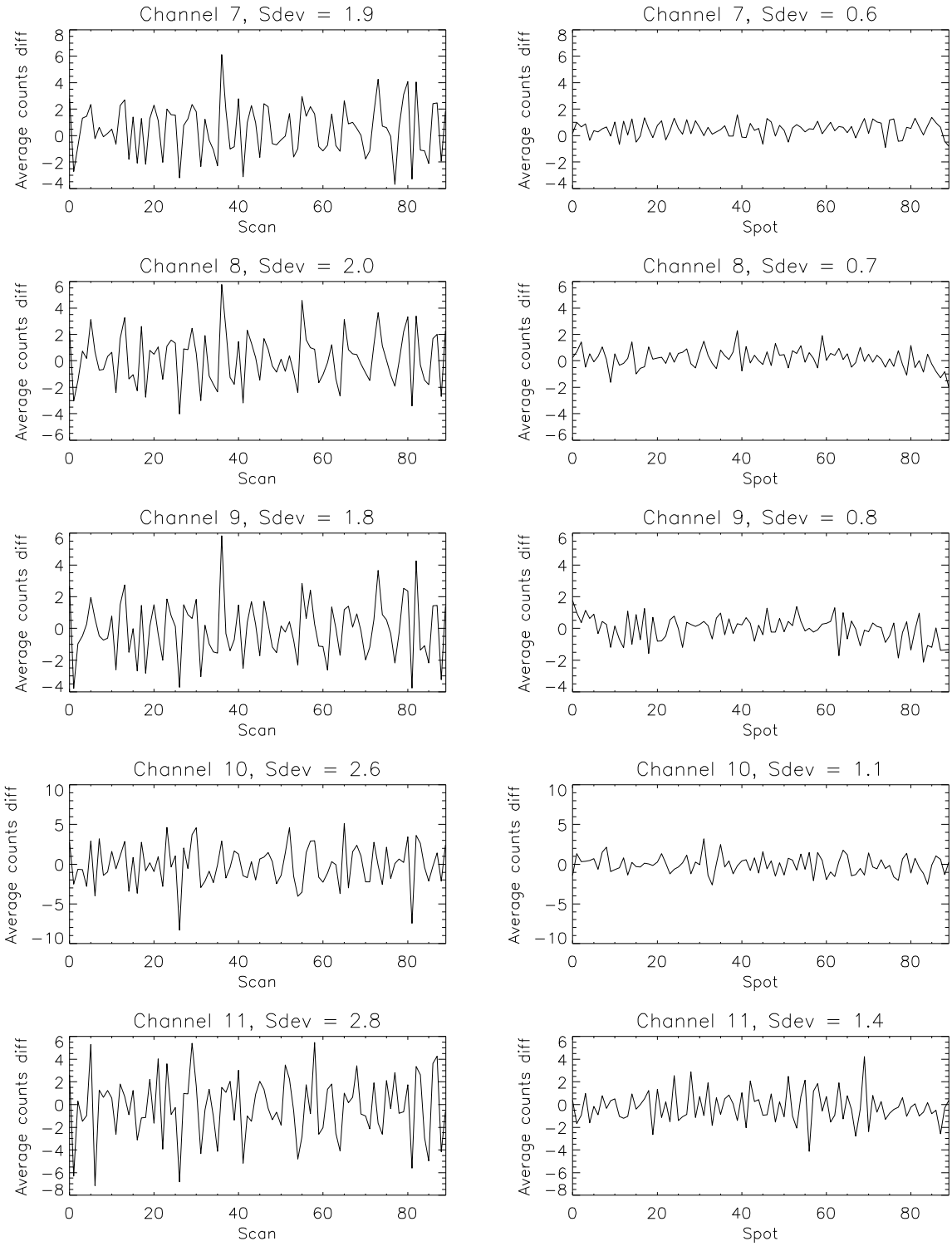

Figure 21: As Fig 19 but using raw counts

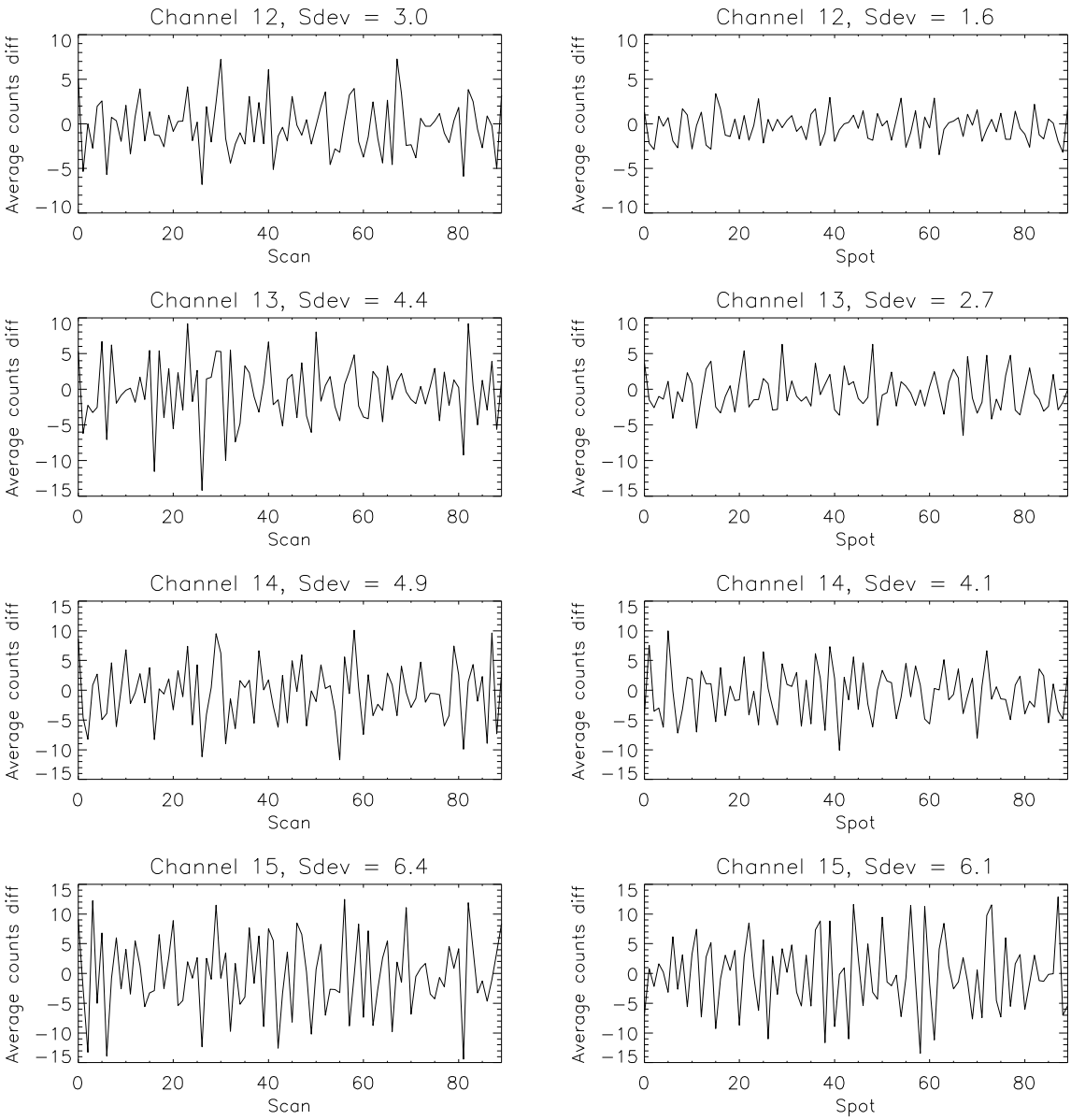

Figure 22: As Fig 20 but using raw counts

2.6.4 Correlation between striping and calibration counts

To investigate the correlations between earth counts, warm counts and cold space counts, the earth scan is divided into groups of 4 pixels (starting at pixel 3) and each group is averaged to create a time series. The cold space counts and warm counts are also averaged. Then each group is selected and the correlation coefficient is calculated between the group and (i) all groups in the earth scan, (ii) space counts, (iii) warm counts and (iv) all groups in the *next* earth scan.

Results for the four central groups of ATMS channels 7, 9 and 14 are shown in Figure 23, Figure 24 and Figure 25 respectively.

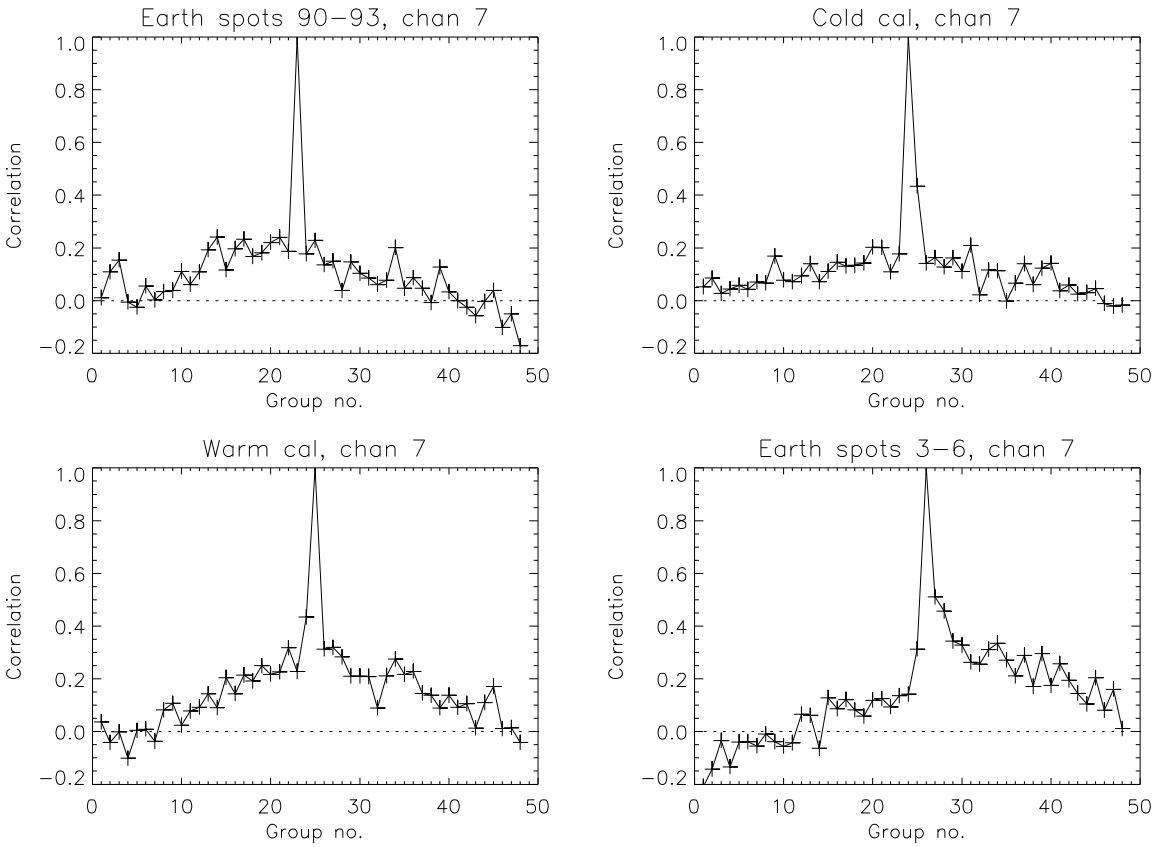

Figure 23: Correlations between groups of 4 pixels for ATMS channel 7. Groups 1-23 are earth views, 24 is cold cal, 25 is warm cal and 26-48 are earth views of the next scan

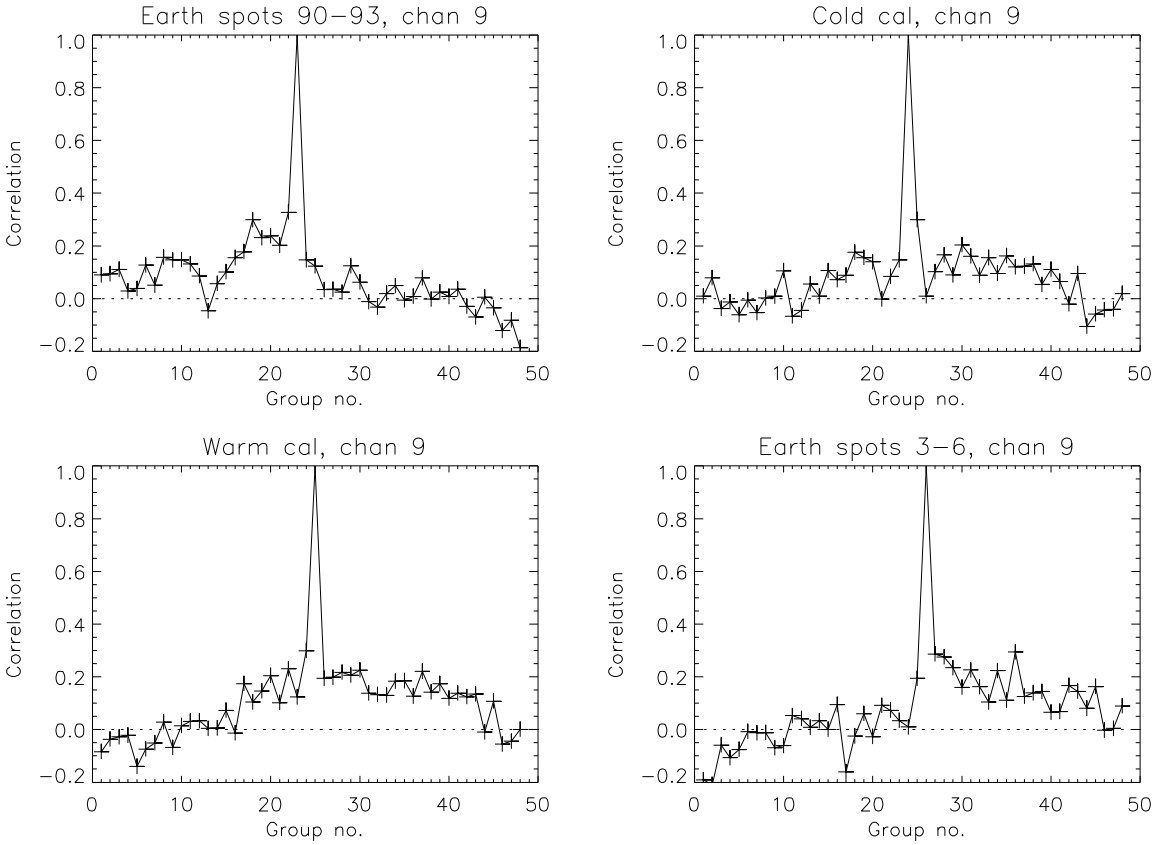

Figure 24: Correlations for channel 9

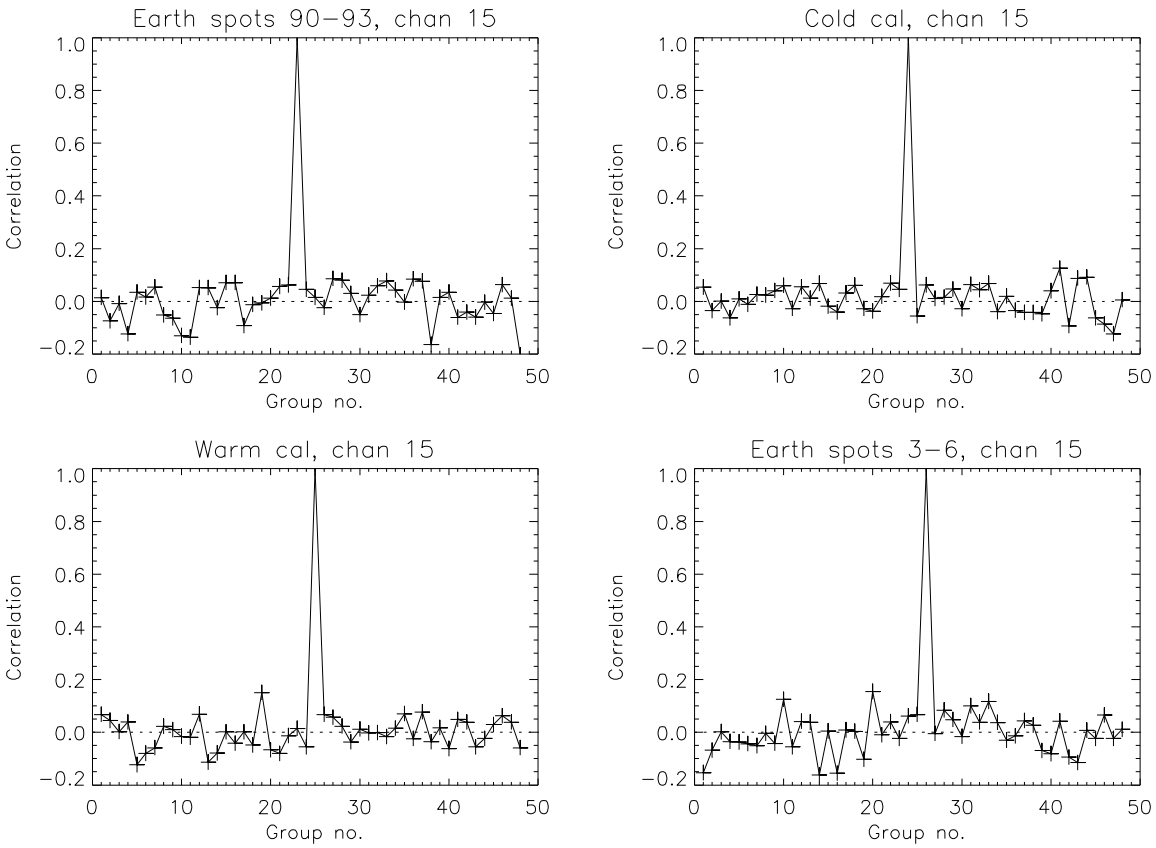

Figure 25: Correlations for channel 15

The plots (including plots for other channels not shown) suggest that for the lower atmospheric sounding channels there are correlations between neighbouring earth views and the calibration views. These correlations extend over many samples, but die away as the time period approaches one scan. The higher numbered channels do not show clear correlations, perhaps because these channels are inherently more noisy.

2.6.5 Inter-channel correlations in the striping

For each pair of channels (7-15), the correlation coefficient was computed between the respective BT difference fields. See Figure 26.

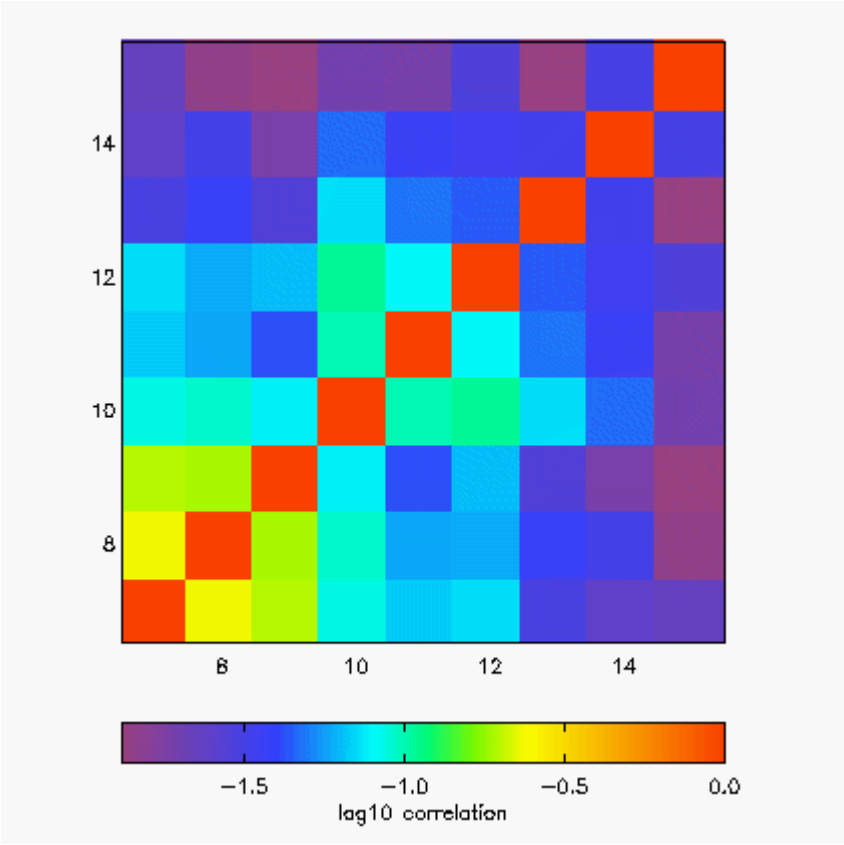

Figure 26: Inter-channel correlations. Note that all correlation coefficients are positive, so can be displayed on a logarithmic scale.

There are significant correlations between the low-number channels, which is consistent with Section 2.6.4 It is also consistent with a study by Niels Bormann (pers. comm.) which used the Desroziers diagnostic. It may be possible to extend this analysis to other channels by choosing a suitable clear-sky sea region.

2.6.6 Contribution of striping to the spatially filtered NEΔT

In section 2.6.2 it was shown that the overall standard deviation of the unfiltered BT difference field is up to 15% larger than the local (4-pixel wide) standard deviation.

The effect of spatial filtering is to reduce the random noise. For example, averaging 3×3 samples reduces random noise by a factor $1/\sqrt{9} = 0.33$. But striping noise is

predominantly in the along-scan direction, therefore is only reduced by a factor $1/\sqrt{3} = 0.58$.

If striping noise and random noise act independently, and can be added in quadrature, then it follows that for the filtered BT field, striping increases the overall noise by a factor of up to 41% – a much larger factor than before remapping. In other words, striping will be more obvious in O-B comparisons that use spatially filtered radiances.

2.6.7 Conclusions of the striping investigation

- Striping artefacts are visible in both the calibrated antenna temperatures and in the earth counts, when a smooth background signal is subtracted.
- There is evidence for inter-channel correlations.
- The noise associated with the striping appears to have a time constant much larger than the ATMS integration time, and therefore is not caused by random noise in the calibration samples. Further investigations (not shown in this report) were performed to investigate the effect of changing the number of calibration samples to be averaged, but it was not possible to achieve any significant reduction in the striping. Similar conclusions were reached in independent investigations at the U.S. Naval Research Laboratory (NRL) (S. Swadley, pers. comm.).
- Striping introduces spatial and spectral correlations, which could be significant for NWP.
- The effect can be reduced somewhat by spatial filtering, at the expense of spatial resolution.
- Striping does not greatly increase the overall noise for unfiltered radiances (<15%), but becomes more prominent, relative to random noise, in spatially filtered data.
- These results are based on a single overpass. Use of more data would increase the robustness.
- It would be interesting to know whether similar effects were seen in pre-launch thermal vacuum data.
- Analysis by NRL of a roll manoeuvre shows that striping is also present in the 23.8, 50.3, 89 and 183 GHz channels. (S. Swadley, pers. comm.)

3. Assimilation Experiments

3.1 Trial set up

The impact of the ATMS data on global analyses and forecasts was tested by adding the ATMS data to a full observing system. The trial covered the period 18th Jan 2012 – 18th Feb 2012. A control experiment was run for this period using a low resolution version of the operational configuration (N320, L70) and development versions of the Observation Processing System (OPS) from 14th February 2012 and the Variational Data Assimilation System (VAR) from 25th June 2012.

The observation error for ATMS for use in both 1D-Var and 4D-Var was calculated by scaling the NOAA-19 values of the **R** matrix by the ratio of the noise given as ATMS *pre-launch specification* and the NEDT for NOAA-19 AMSU (Table 2), except for the 183 GHz channels for which **R** was set to 4 K. For channel 4, which has no counterpart on AMSU the value was obtained by interpolation between the values for channel 3 and channel 5.

An additional trial was also run with **R** values for all channels that were less than 0.35 K increased to 0.35 K. The observation errors were inflated in this manner to take account of the striping problem described in Section 2.6. The two trials will be referred to as the *normal R trial* and the *inflated R trial*. Table 4 shows the observation errors used in 1D- and 4D-Var in each trial.

Table 4: Square root of the observation errors (diagonal R matrix values) used in 1D-Var in the two trials

ATMS channel	Normal R trial values (K) (1D-Var)	Inflated R trial values (K) (1D-Var)	Normal R trial values (K) (4D-Var)	Inflated R trial values (K) (4D-Var)
1	9.19	9.19	12.25	12.25
2	5.88	5.88	14.00	14.00
3	2.68	2.68	2.45	2.45
4	1.95	1.95	2.33	2.33
5	1.23	1.23	2.21	2.21
6	0.30	0.35	0.38	0.38
7	0.23	0.35	0.38	0.38
8	0.26	0.35	0.33	0.35
9	0.33	0.35	0.66	0.66
10	0.55	0.55	0.55	0.55
11	0.98	0.98	0.65	0.65
12	0.90	0.90	0.75	0.75
13	1.10	1.10	1.23	1.23
14	0.89	0.89	1.81	1.81
15	1.28	1.28	5.13	5.13
16	8.00	8.00	8.00	8.00
17	4.33	4.33	4.33	4.33
18	4.00	4.00	4.00	4.00
19	4.00	4.00	4.00	4.00
20	4.00	4.00	4.00	4.00
21	4.00	4.00	4.00	4.00
22	4.50	4.50	4.50	4.50

The ATMS channels used in the trial were 6-15 and 18-22. Surface sensitive channels were omitted. The quality control (QC) checks were set following the treatment of AMSU data. The data are sufficiently similar that this should screen low quality ATMS observations. There are four flags applied to screen out observations in the presence of deep cloud and precipitation as radiative transfer in these conditions is less reliable. These are termed ‘rain’, ‘bennartzrain’, ‘mwbcloudy’ and ‘mwcloudy’.

The ‘rain’ flag is a scattering test on the 89, 23 and 31 GHz channels, the ‘bennartzrain’ flag is an additional scattering index based on 89 and 150 GHz. The ‘mwbcloudy’ flag, also known as a cirrus cost test, uses the 183 GHz AMSU channels. The ‘mwcloudy’ test is carried out in AAPP and identifies areas of high liquid water path and categorises the most likely surface type for a field of view. All of these tests are described in more detail in Appendix 1.

ATMS channels 7, 8, 9, 21 and 22 are rejected when flags 'rain' and ‘bennartzrain' are set. Channels 19 and 20 are rejected when the ‘mwbcloudy’ flag is set and channels 6 and 18 are rejected when the ‘mwcloudy’ flag is set.

Table 5 is taken from the OPS output and summarises the channel selection for the trial

Table 5: ATMS channel selection

Flag/ATMS channel	6	7	8	9	10	11	12	13	14	15	18	19	20	21	22
Clear	+	+	+	+	+	+	+	+	+	+	+	+	+	+	+
Mwbcloudy	+				+	+	+	+	+	+	+				
Mwcloudy					+	+	+	+	+	+					
Rain	+				+	+	+	+	+	+	+	+	+		
Bennartz rain	+				+	+	+	+	+	+	+	+	+		
Sea	+	+	+	+	+	+	+	+	+	+	+	+	+	+	+
Seaice		+	+	+	+	+	+	+	+	+					
Land		+	+	+	+	+	+	+	+	+					
Highland			+	+	+	+	+	+	+	+					
Mismatch			+	+	+	+	+	+	+	+					

3.2 Trial results

At the Met Office an index known as the *NWP index* is used to evaluate changes to the forecast assimilation and processing system, this index is a weighted combination of different analysis statistics obtained by comparing and experiment, or trial, including the change with a control. Further details of the NWP index can be found in Appendix A of Rawlins *et al.* (2007). The headline NWP index statistics for the two trials compared with the control are shown in Table 6. Results are neutral, with the inflated R trial slightly more negative, except for global change against observations where inflated R is slightly more positive than the normal R. However, the differences are minimal and the impact with respect to the NWP index for both trials is firmly neutral.

Table 6: Impact on NWP Index. Positive numbers represent an improvement.

Trial	NWP index change against observations (absolute change and expressed as a percentage)				NWP index change against analysis
	Global	NH	Tropics	SH	Global
Normal R	0.136 0.104%	0.006 0.03%	-0.069 -1.05%	-0.078 -0.46%	0.064 0.042%
Inflated R	0.154 0.118%	-0.002 -0.01%	-0.102 -1.55%	-0.001 0.00%	-0.203 -0.132%

Figure 27 shows the mean RMS change and the change in weighted skill for the normal R trial and Figure 28 shows the same for the inflated R trial, against observations and analysis. In general, for both trials against observations and against analysis, an improvement in seen in the Northern Hemisphere and the Southern Hemisphere. In the Southern Hemisphere mean sea level pressure (PMSL) and 500 hPa height (H500) are initially degraded at T+24, but this gives way to an increase in skill at longer forecast ranges indicating a possible improvement from the ATMS observations, i.e. the increase in bias comes from true changes in structure.

In the Tropics the picture is generally negative. A small improvement in RMSE against observations is seen in the tropics in both experiments, but there is no corresponding increase in the skill for the 850 hPa winds. This is unexpected and unexplained and may indicate a problem with the verification. Against analysis the signal is more consistent, with an increase in RMSE and a decrease in skill. The apparent degradation in tropical scores against analysis is most likely due to a change in structure in tropical moisture fields (and hence winds) from the five ATMS 183 GHz channels, which is quickly lost in the forecast. In this situation the RMS errors appear to be increased as a consequence of enhanced variability in the verifying analysis. This aspect requires further investigation.

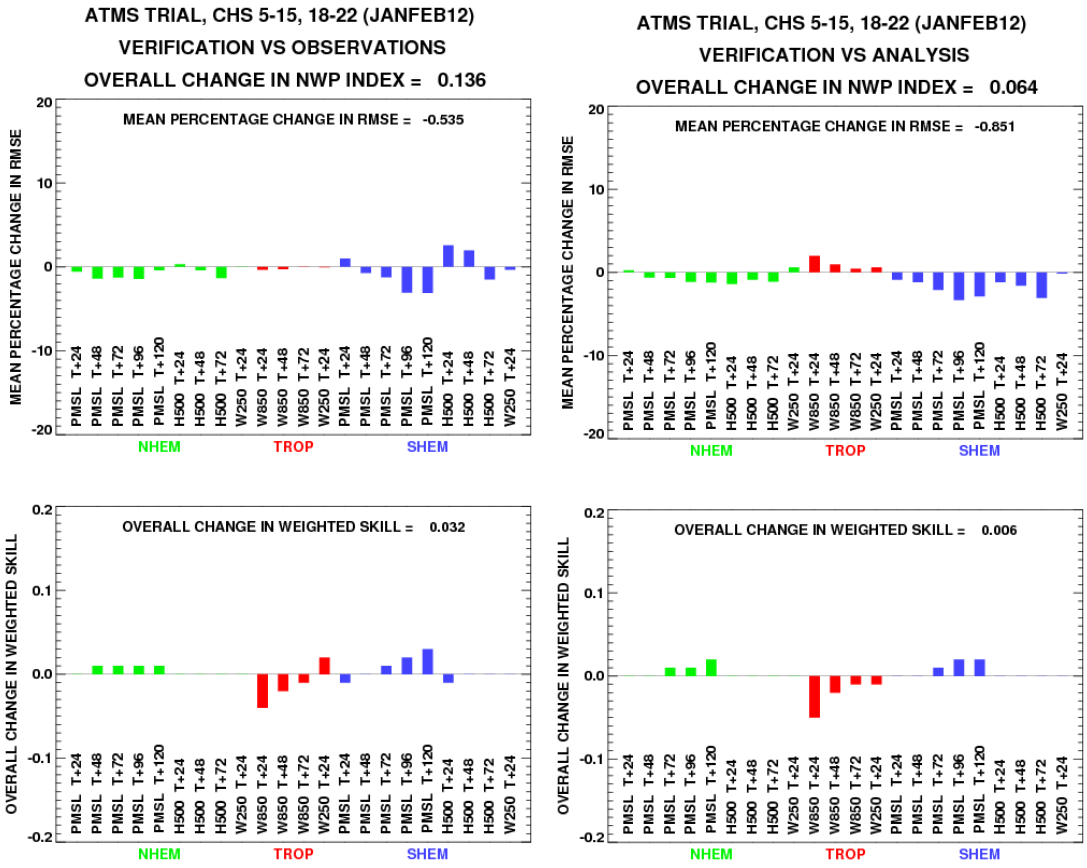

Figure 27: mean RMS change and change in weighted skill for observations and analysis for the normal R trial

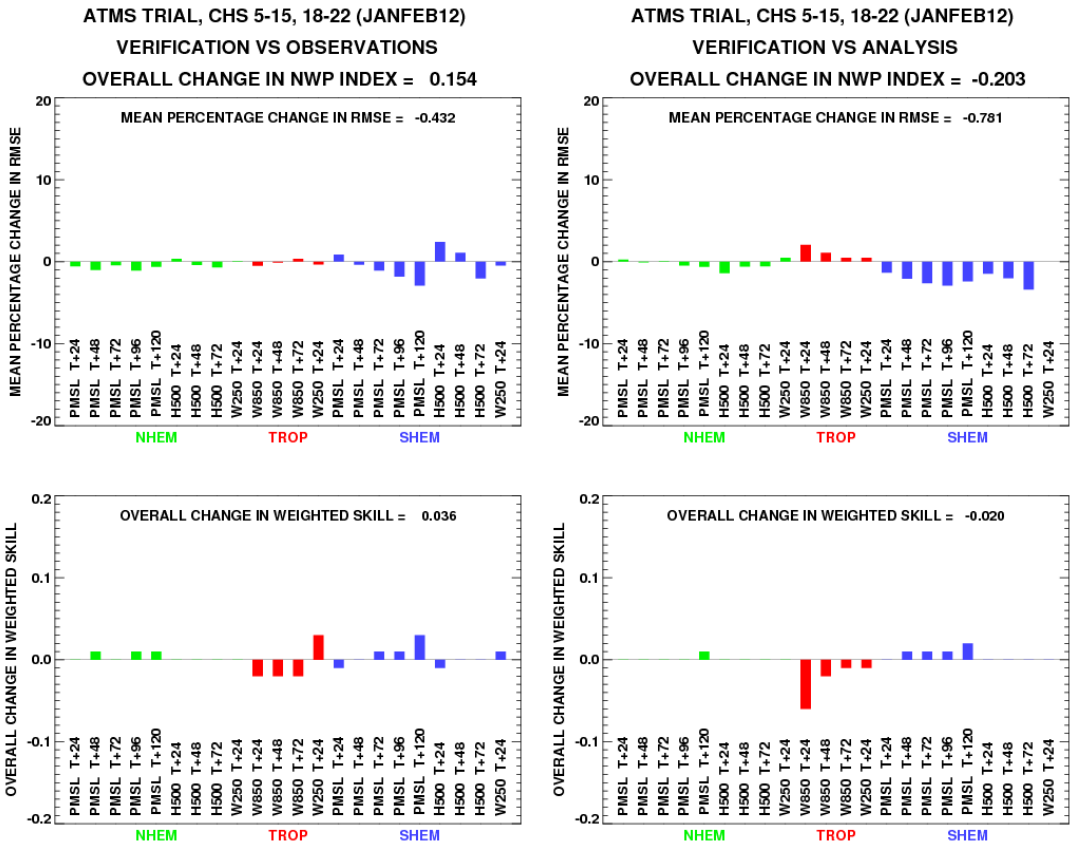

Figure 28: mean RMS change and change in weighted skill for observations and analysis for the inflated R trial

3.2.1 Background fits to observations: sondes

Figure 29 shows the time series of mean and RMS error for sonde 500 hPa geopotential height for the normal R trial. There is an increase in mean error of magnitude ~0.5 m throughout the trial period. At 500 hPa geopotential height the altitude is ~5000 m, so this increase is roughly 1 part in 10^4, this compares well with the residual local biases of ~30 mK in 300 K which are of the same order. The degradation is still evident at T+24, but the magnitude of the change is smaller, again suggesting an initial change in structure from the ATMS observations that does not persist through to longer forecast ranges.

Figure 30 shows the mean and RMS values against sonde observations and against analysis for the 500 hPa temperature for increasing forecast range. A warm bias of ~50 mK relative to control persists across the forecast ranges against observations. Both control and trial show a cold bias relative to analysis with the ATMS cold bias ~20 mK worse than the control.

Model level 29 is at roughly 500 hPa over sea. For the normal R trial Figure 31 shows the mean differences with sonde theta observations at this level for the last iteration in 4D-Var, equivalent to forecast minus analysis values (O-A). This figure shows that the warm bias relative to control shown in Figure 30 also persists throughout out the trial period. There were no significant differences in RMS.

The inflated R trial was very similar to the normal R trial for all of these plots.

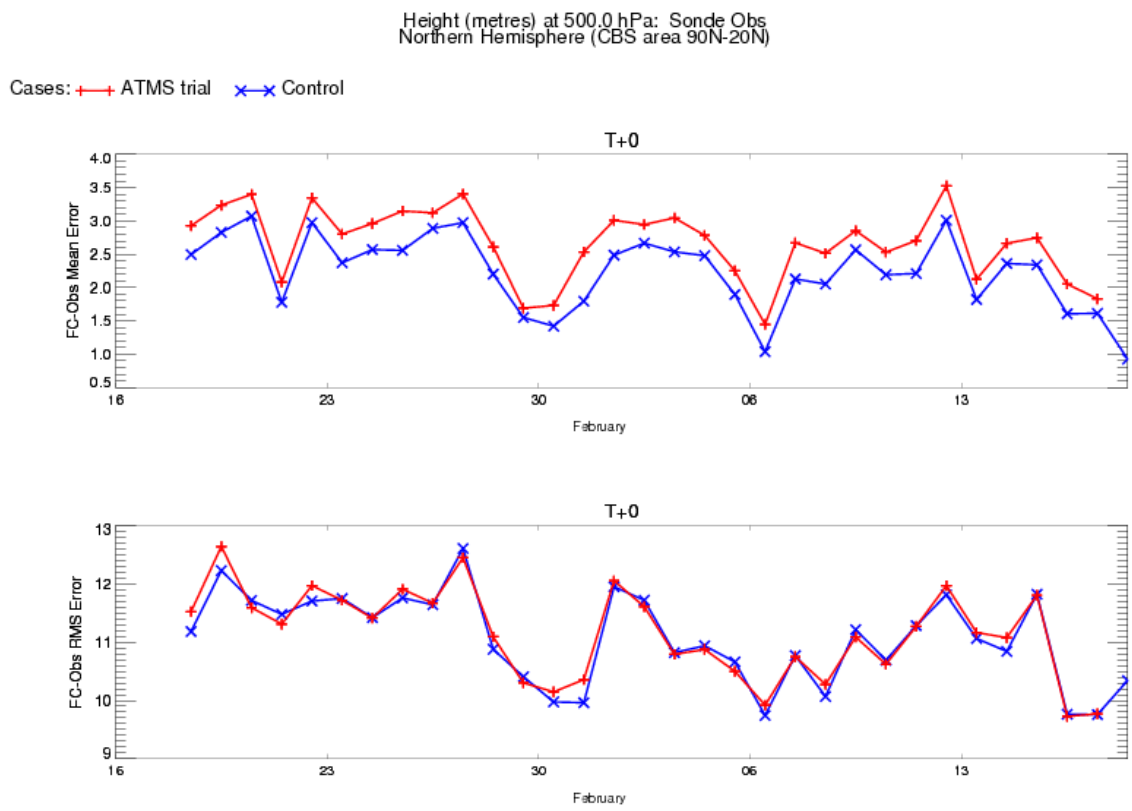

Figure 29: normal R trial, time series of mean (top) and RMS (bottom) T+0 analysis minus sonde observations at 500 hPa.

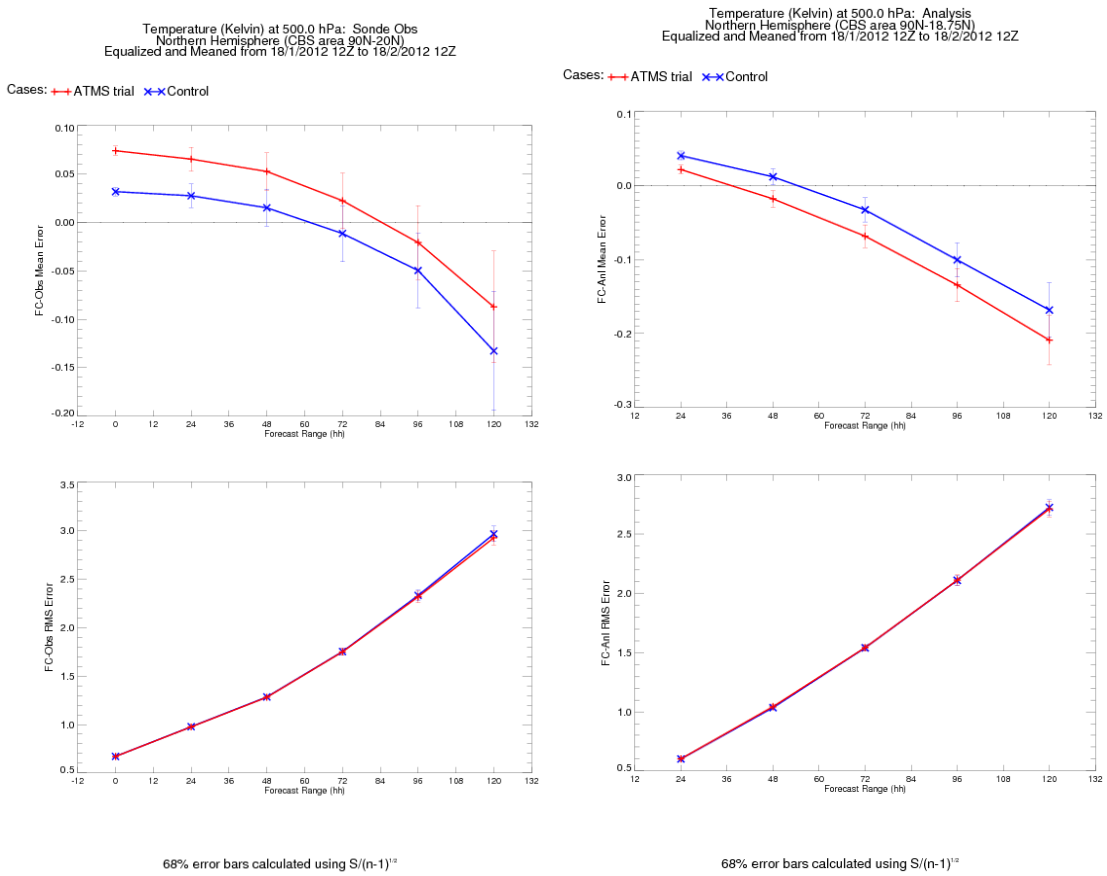

Figure 30: Normal R trial, mean (top) and RMS (bottom) of 500 hPa temperature forecast minus sonde observation (left) and forecast minus analysis (right)

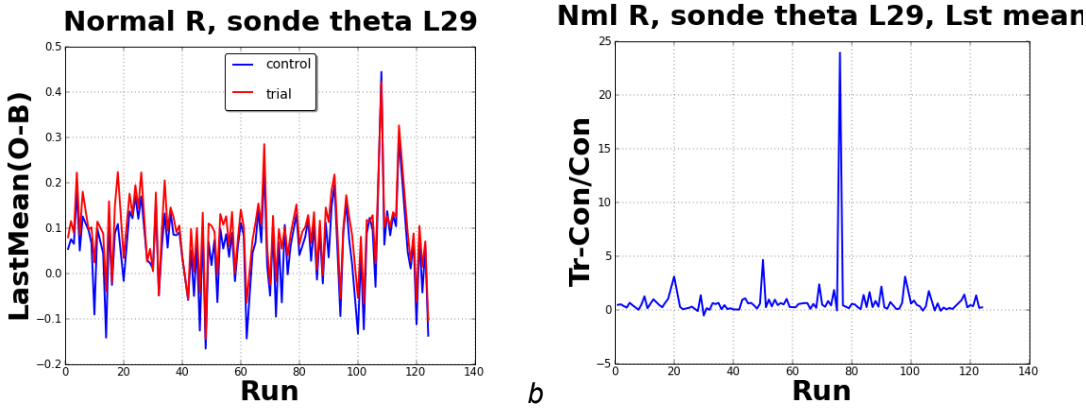

a *b*

Figure 31: Mean O-B for sonde theta at level 29 for the last iteration of VAR. a) O-B for control and normal R trial, b) difference between trial and control as a fraction of control value.

3.2.2 Background fit to observations: ATOVS

Background fits for AMSU were investigated by examining the O-B values at the start of 4D-Var and at the end (analogous to observation minus analysis (O-A)). Figure 32 shows the RMS of the O-B for Metop-A AMSU channel 8. There is a pronounced improvement in trial compared to control for both the inflated and the normal R. Similar

impact can also be seen in channels 5, 7, 9 and 14 in most of the ATOVS instruments. Indicating that ATMS improves fit to AMSU. However, AMSU channel 6 shows consistently worse mean and RMS when ATMS is included, for all instruments. The higher peaking temperature sounding channels (AMSU channels 10-14) show no impact or negative impact. Of interest is RMS in the higher sounding channels (10-14) which has a monotonic decrease in value across the time period for all satellites and all channels, this is possibly due to a drift in bias across the period of the trial. An example of this is shown in Figure 33.

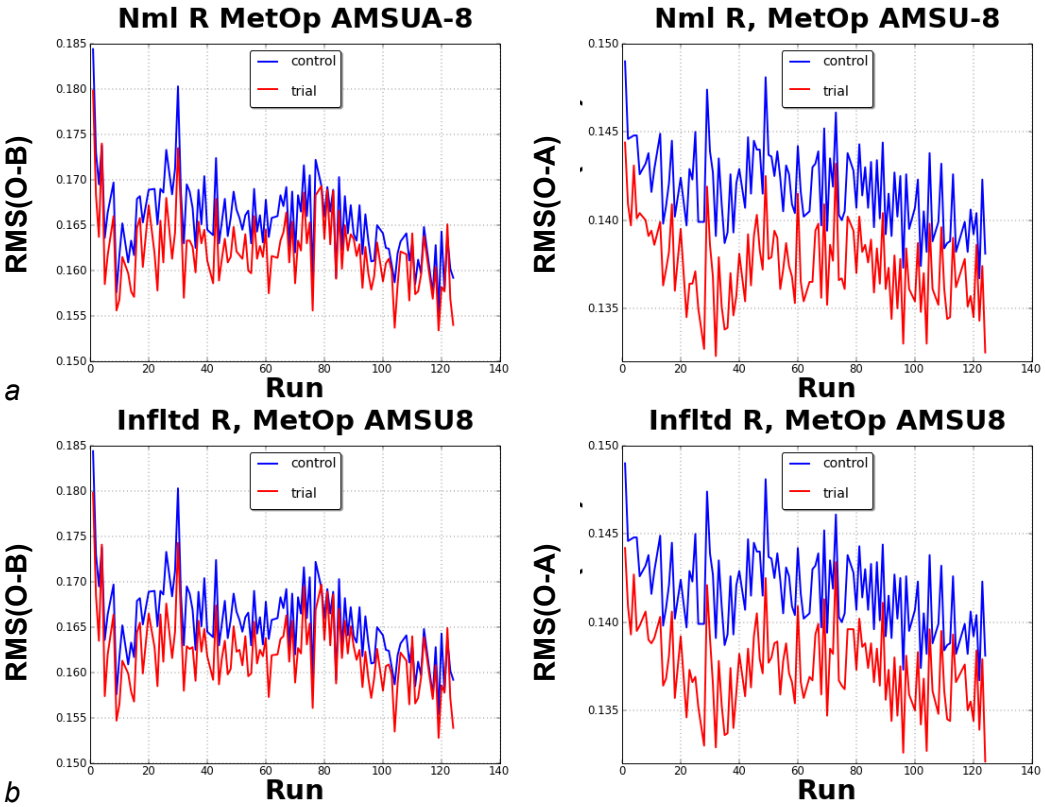

Figure 32: a) normal R trial and b) inflated R trial: first RMS O-B (left) and last RMS O-B or O-A (right) for Metop AMSU channel 8 for control and trial

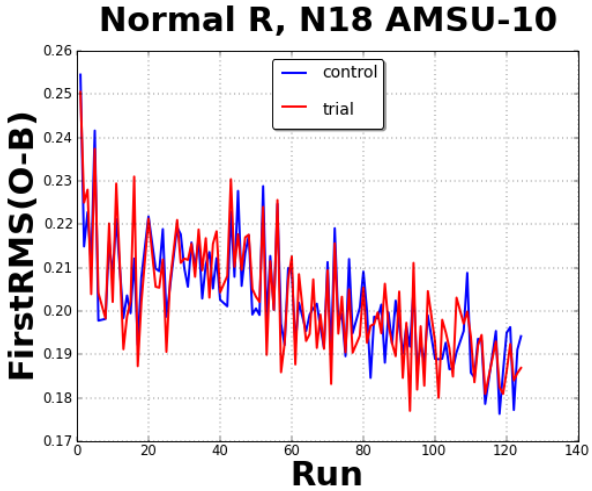

Figure 33: NOAA 18 AMSU channel 10 showing the monotonic decrease in RMS for both trial and control across the trial period, this is seen in channels 10-14 for all instruments.

Figure 34 shows the RMS of O-B for the first 4D-Var iteration (O-B) and for the last iteration (O-A) for NOAA 19 AMSU channel 6. As mentioned above, AMSU channel 6 shows degradation when ATMS is added, unlike other channels. This degradation is also seen in the mean values (not shown). One reason for this may be an error in the quality control for ATMS channel 6 during these trials (Table 5), allowing ATMS channel 6 to be assimilated in the presence of rain. This requires further trialling with the correct treatment of ATMS channel 6.

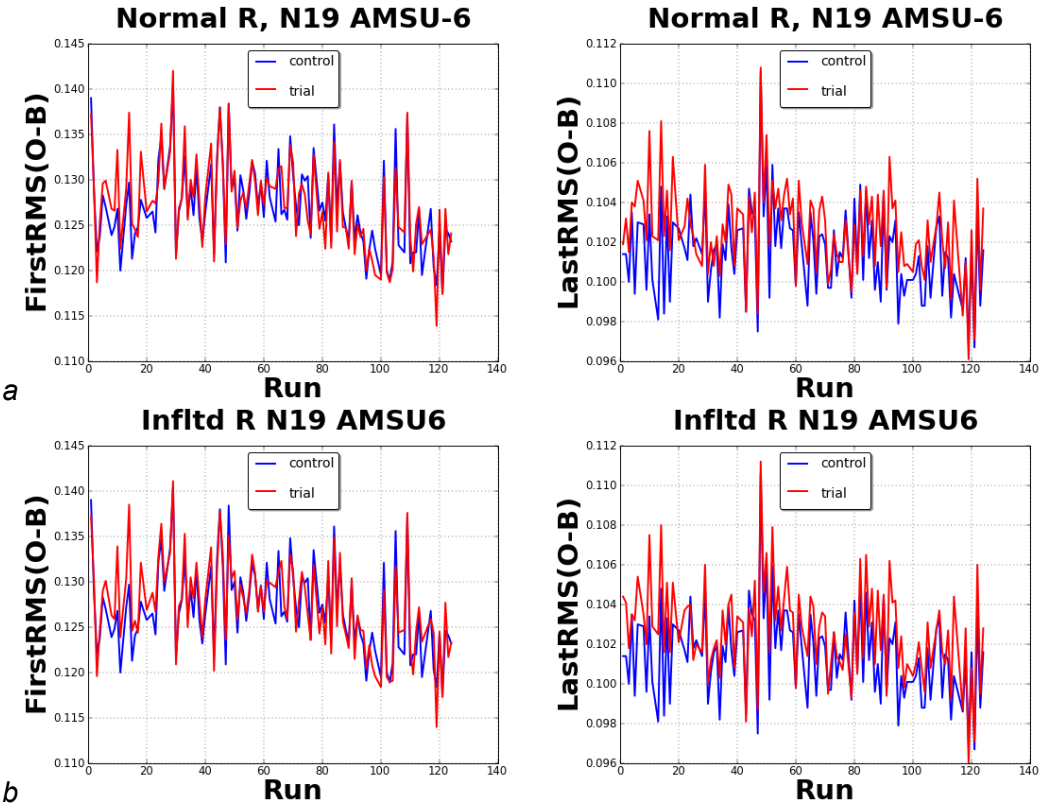

Figure 34: a) normal R trial and b)inflated R trial: first(left) and last (right) RMS O-B for NOAA19 AMSU channel 6 for control and trial

3.2.3 Background fit to observations: IASI

IASI channels 75, 81 and 170 were chosen for the investigation as these channels are used to monitor IASI data at the Met Office and all are assimilated, channel 75 is used under all conditions and over all surfaces, channel 81 in all conditions over sea and sea ice, and channel 170 only in sea and clear conditions. Some details of these channels are shown in Table 7 (source, P.Weston, pers. comm.).

Table 7: Characteristics of the IASI channels examined in the analysis

IASI channel	Central wavenumber	T jacobian peak (hPa)	T jacobian peak (km)
75	706.25	339.39	8.65
81	711.00	436.95	6.87
170	1204.50	899.69	1.30

Figure 35, 36 and 37 show IASI channels 75, 81 and 170 respectively. Channel 81 (Figure 36) is of most interest as this peaks closest to 500 hPa. All three channels have reduced RMS in the trial compared to the control. All plots are for the normal R trial, the inflated R trial is similar.

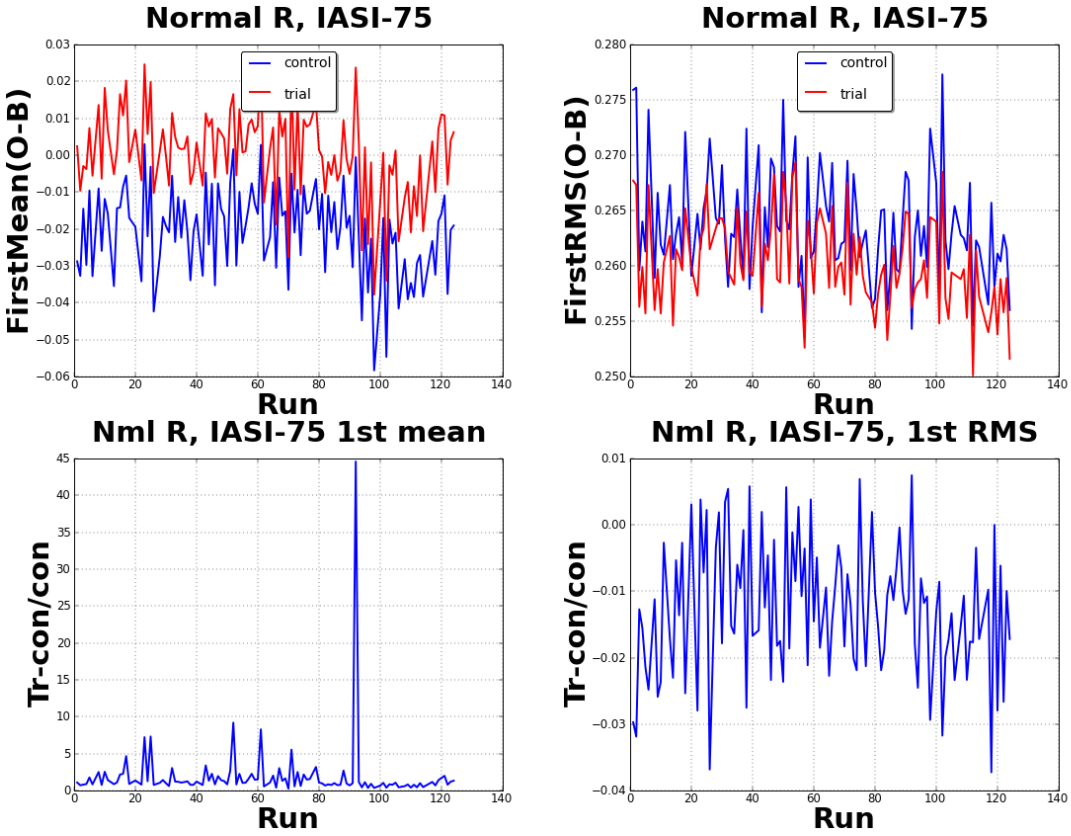

Figure 35: IASI channel 75 first VAR iteration mean(left) and RMS (right) for the normal R trial. Top row is control and trial values, bottom row is the difference between trial and control as a fraction of the control value.

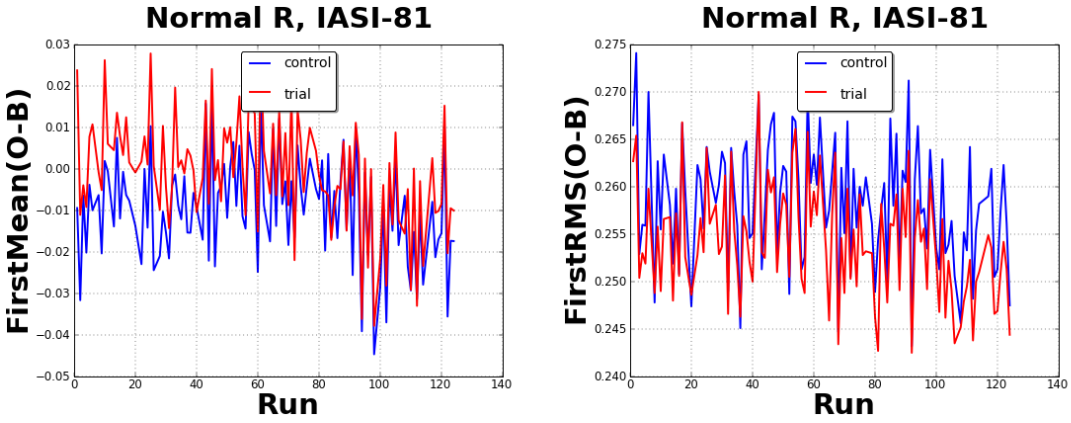

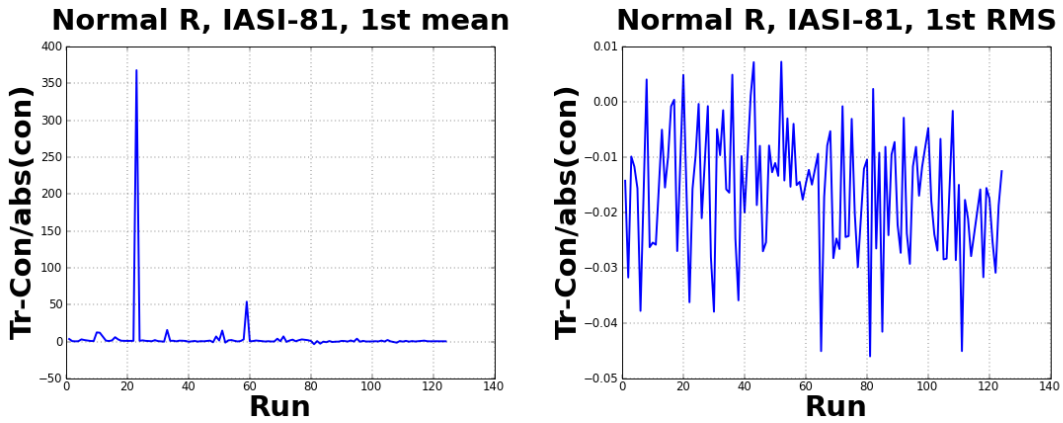

Figure 36: IASI channel 81 first VAR iteration mean(left) and RMS (right) for the normal R trial. Top row is control and trial values, bottom row is the difference between trial and control as a fraction of the control value.

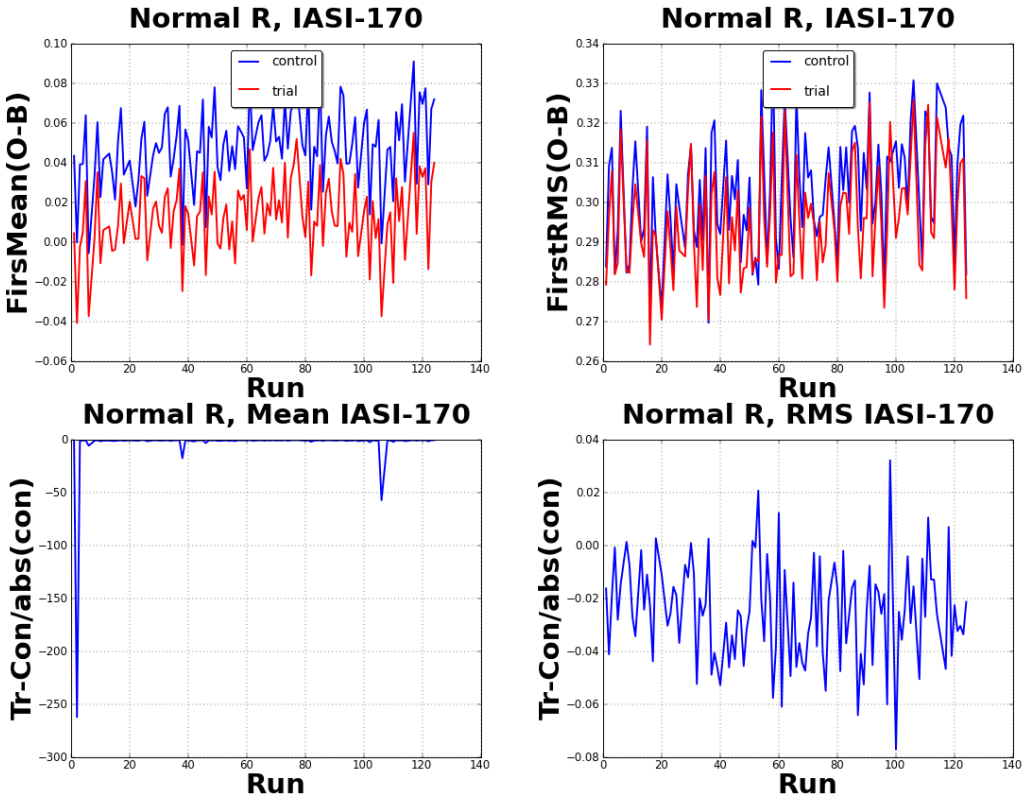

Figure 37: IASI channel 170 first VAR iteration mean(left) and RMS (right) for the normal R trial. Top row is control and trial values, bottom row is the difference between trial and control as a fraction of the control value.

3.2.4 Examination of second half of trial period only

From the plots in Figure 6 and 7 it appears that there is a marked decrease in variability in the RMS values for the second half of the trial, from 2nd February onwards, there also are fewer data dropouts and more consistent observation counts for this later period (Figure 7). Examining verification for the last 17 days of the trial (02/02 to 18/02) showed much improved performance, although for such a short period results are not robust,

especially for longer forecast ranges. Table 9 shows the headline stats for this shortened trial period for both normal R and inflated R.

Table 9: Headline statistics second half of trial period

Trial	NWP index change against observations				NWP index change against analysis	
	Global	NH	Tropics	SH	Global	
Normal R	0.487	0.017	-0.049	-0.099	1.128	0.720%
trial	0.369%	0.09%	-0.7%	-0.60%		
Inflated R	0.573	0.026	-0.139	-0.053	0.579	0.370%
trial	0.434%	0.13%	-1.99%	-0.32%		

The impact on the global NWP index is now positive against both analysis and observations, although the impact against observations in all of the three latitude bands is still neutral and actually worse in the SH than for the verification for the whole period of the trial.

Figure 38 shows the the mean RMS change and the change in weighted skill for the normal R trial and Figure 39 shows the same plot for the inflated R trial, against observations and analysis.

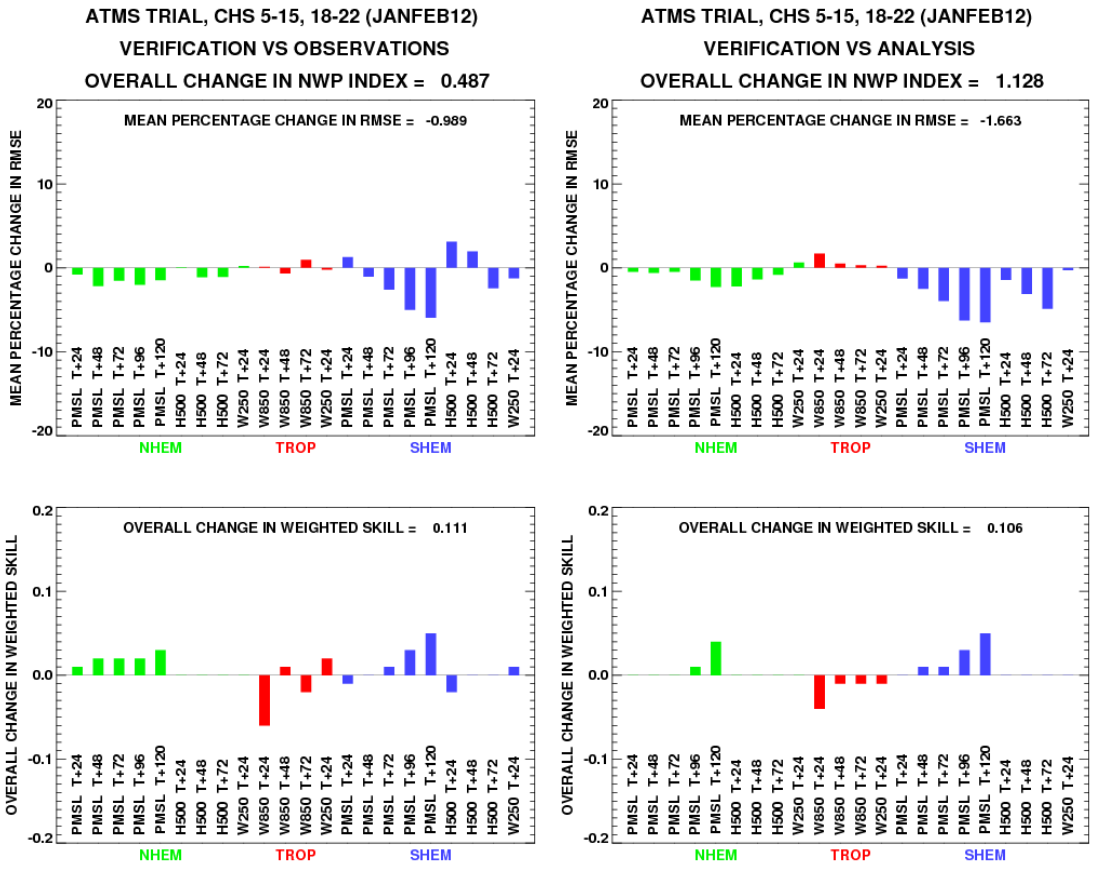

Figure 38: mean RMS change and change in weighted skill for observations and analysis for the reduced time period, normal R trial

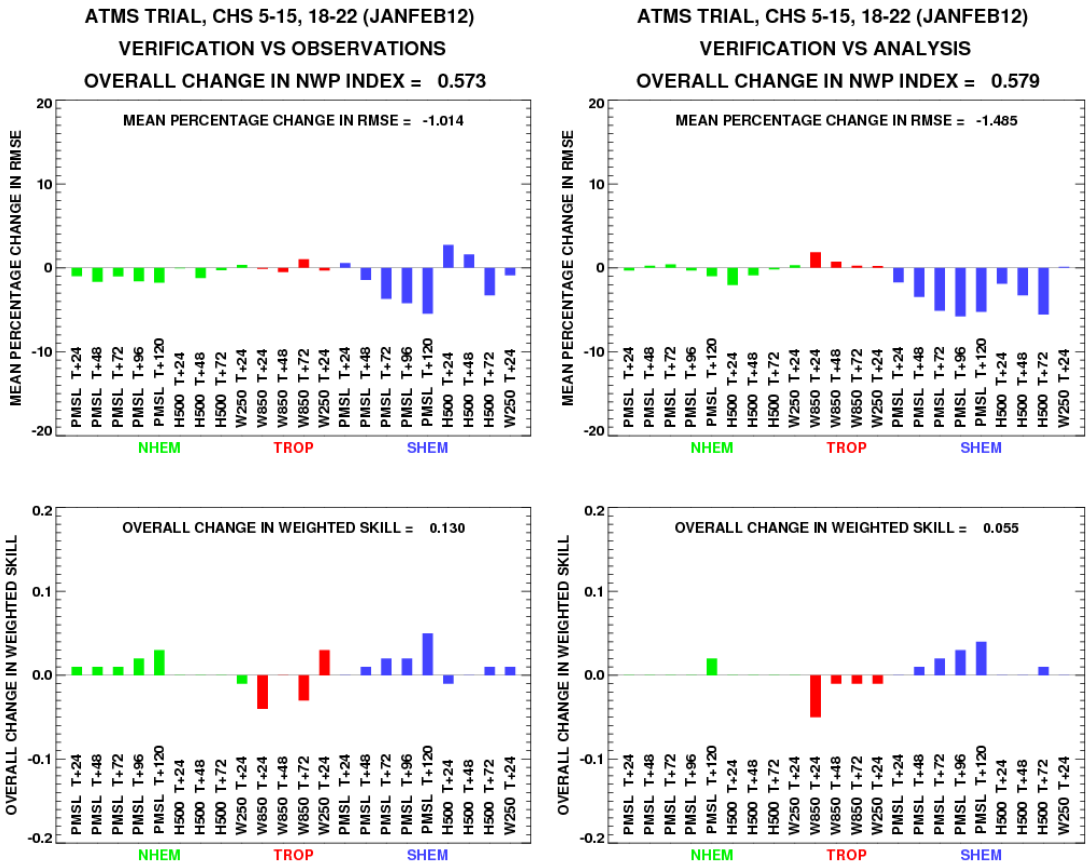

Figure 39: mean RMS change and change in weighted skill for observations and analysis for the reduced time period, inflated R trial

3.2.5 Resource considerations

OPS was run on a full node and the time taken from after the MetDB extraction to end of processing was calculated. This was done four times, the results are shown in Table 8. The average value is 48 seconds.

Table 8: Time taken for ATMS in OPS on one node

Date	Number of obs processed	Timestamp at start of OPS job	Timestamp at end of MetDB extract	Timestamp at end of OPS job	Time taken (s)
12 September 2012 QU12	64896	09:21:39	09:21:49	09:22:44	55
12 September 2012 QU18	62976	09:25:27	09:25:37	09:26:31	54
13 September 2012 QU00	57760	06:30:37	06:30:47	06:31:37	50
13 September 2012 QU06	21856	09:28:23	09:28:29	09:29:02	33

For the JanFeb12 trial the number of iterations increased from 20 in the control to 39 in the ATMS trial. For the JunAug12 the number of iterations was 30 in both the control and the ATMS trial.

4. Conclusions and Future work

An initial assessment of ATMS data from January and February 2012 together with ATMS data received in near real time after 26th June 2012 has been carried out. This assessment has involved an inspection of innovations and innovation statistics, together with comparisons with AMSU and MHS data.

The effective radiometric performance of the remapped ATMS data is expected to be excellent as a result of the remapping applied to match the effective ground footprint with that of AMSU-A. Based on the warm load and cold space views the *effective* NEΔT, after remapping, is in the range 60-100 mK for the key lower atmospheric temperature sounding channels (6-10). This compares favourably with the equivalent figures for AMSU-A on Metop-A and NOAA-19 which are the range 160-180 mK.

Despite this performance advantage over AMSU (as currently processed in the Met Office systems) the standard deviations of bias corrected innovations for most of the temperature sounding channels (6-15) are slightly worse than for AMSU-A equivalents. The most likely reason for this is that a *striping effect* evident in the ATMS observations is contributing to the variance in the innovations. The mechanisms causing this striping are under investigation by the Cal/Val team. It is likely that the amplitude of the striping effect, at several tenths of a Kelvin, is sufficiently large to adversely affect the impact of the ATMS data in the assimilation and forecasting system.

For the humidity sounding channels examined (183±1, ±3, ±7 GHz – channels 18, 20 and 22) the performance of ATMS is very close to that of AMSU-B / MHS. For the surface viewing channels (1-3, 5, 16 and 17) the ATMS data shows slightly larger bias and standard deviation.

Two assimilation experiments were conducted in which ATMS was added to a full Met Office system. In the first the assumed observation errors were obtained by scaling those for NOAA-19 by the ratio of the pre-launch specified NEΔT for ATMS to that for NOAA-19 on-orbit. In addition to this experiment ('*normal R*') an experiment was carried out in which observation errors for the lower atmospheric sounding channels were increased to a minimum of 0.35 K. For both experiments ('*normal R*' and '*inflated R*') the impact on global forecasts was found to be neutral. In the Northern and Southern Hemispheres the results were neutral, while in the tropics negative results were seen which require further investigation.

Further investigations into these assimilation experiments showed that the data volume over the period (Jan-Feb 2012) was highly variable during the first half of the trial period. During the second half of the trial period data volumes were much more stable. When verified over the last 17 days of the Jan/Feb trial the results appear to be more positive although no conclusions can be drawn from a trial over such a short period.

Priorities for future work on ATMS will focus on:

- Performing assimilation experiments over a second season (Summer 2012) to assess the impact of ATMS data on analyses and forecasts, using the conservative channel selection and assumed observation errors described in this report. ATMS data will be included in the next Met Office operational upgrade (Parallel Suite 32), currently due to be implemented in November 2012.

- Investigations into the striping effect aimed at characterising the problem, elucidating likely causes and contributing to the development of correction strategies in collaboration with the wider ATMS Cal/Val team.

- Carrying out further assessments of data quality, following updates to the bias correction and improvements in the handling of the striping effect.

- Further improvements to the bias corrections and data screening to better deal with the large biases evident at high southern latitudes in many of the high peaking temperature sounding channels.

- Further tuning of the assumed observation errors, based on advanced diagnostics as well as empirical *ad-hoc* tuning of the **R** matrix.

- Studying the impact of a more aggressive use of the low peaking temperature sounding channels, using a physically based error model recently developed for AMSU-A channels 4 (52.8 GHz) and 5 (53.6 GHz). Eventually, if improvements in the use of AMSU channels 1 and 2 can be achieved then similar channel selections will be evaluated in the operational use of ATMS

- Evaluating options for the use of the 183 GHz channels.

References

Bell, W., Di Michele, S., Bauer, P., McNally, T., English, S. J., Atkinson, N., Hilton, F. and Charlton, J., 2010: The Radiometric Sensitivity Requirements for Satellite Microwave Temperature Sounding Instruments for Numerical Weather Prediction. *Journal of Atmospheric and Oceanic Technology*, **27:** Issue 3, 443-456.

Bennartz, R., Thoss, A., Dybbroe, A. and Michelson, D.B., 2002: Precipitation analysis using the Advanced Microwave Sounding Unit in support of nowcasting applications. *Meteorol. Appl.* **9**: 177-189.

Harris, B. A. and Kelly, G., 2001: A satellite radiance-bias correction scheme for data assimilation. *Quarterly Journal of the Royal Meteorological Society*, **127**: 1453–1468.

Goodrum, G., Kidwell, K. B. and Winston, W. (eds.), 1999: NOAA KLM User's Guide. NOAA, NOAA-NESDIS/NCDC, Suitland, Maryland, USA. Available at http://www.ncdc.noaa.gov/oa/pod-guide/ncdc/docs/klm/index.htm.

Lu, Q., Bell, W., Bauer, P., Bormann, N. and Peubey, C., 2010: An Initial Evaluation of FY-3A Satellite Data, *ECMWF Research Department Technical Memorandum No. 63.* ECMWF, Shinfield Park, Reading, UK. ECMWF. Available at : http://www.ecmwf.int/publications/library/do/references/show?id=89899

Lu, Q., Bell, W., Bauer, P., Bormann, N. and Peubey, C., 2011: Characterizing the FY-3A Microwave Temperature Sounder Using the ECMWF Model, *J. Atmos. Ocean. Tech.,* **28**: 1373-1389.

Marburger, J. H., 2010: Restructuring the National Polar-orbiting Operational Environmental Satellite System, *White House Office of Science and Technology Policy Fact Sheet*, 2011 R&D Budget Submission.

Muth, C., Lee, P.S., Shiue, J.C. and Allan Webb, W., 2004: Advanced Technology Microwave Sounder on NPOESS and NPP. *Geoscience and Remote Sensing Symposium, 2004.* IGARSS '04. Proceedings.

NWP SAF, 2011a: Annex to AAPP scientific documentation: Pre-processing of ATMS and CrIS, document NWPSAF-MO-UD-027. Available at http://research.metoffice.gov.uk/research/interproj/nwpsaf/aapp/index.html

NWP SAF, 2011b: AAPP documentation scientific description, document NWPSAF-MF-UD-001. Available at http://research.metoffice.gov.uk/research/interproj/nwpsaf/aapp/index.html

Rawlins, F., Ballard, S. P., Bovis, K. J., Clayton, A. M., Li, D., Inverarity, G. W., Lorenc, A. C. and Payne, T. J., 2007 : The Met Office global four-dimensional variational data assimilation scheme, *Q. J. R. Meteorol. Soc.* 133: 347–362.

Sreerekha, T.R., Doherty, A. M., English, S.J., Rayer, P. J., 2008 : Potential of Microwave Sounder 229 GHz Channel. *Final Report, EUMETSAT Contract No. EUM/CO/07/4600000409/CJA*.

Appendix 1

A1.1 Scattering test ('rain' flag)

AMSU channel 15 brightness temperature (BT) is calculated using channels 1,2 and 3 (estimated BT = EBT) (Equation A1). Differences between the estimated and observed BT_{15} are attributed to scattering by ice and assigned as the value of a scattering index (SI) (Equation A2).

$$EBT_{15} = a + bBT_1 = cBT_2 + dBT_3 \quad \text{A1}$$

Coefficients *a, b* and *c* are functions of the scan angle.

$$SI = EBT_{15} - BT_{15} \quad \text{A2}$$

This test is applied over sea only and a field of view is flagged as cloudy when

$$|SI| > 10\ K \quad \text{A3}$$

Source AAPP Science document
(**http://research.metoffice.gov.uk/research/interproj/nwpsaf/aapp/index.html**)

A1.2 Bennartz test ('bennartzrain' flag)

The Bennartz rain test is a scattering index of the form

$$SI = TB_{89GHz} - TB_{150GHz} - offset \quad \text{A4}$$

Where

$$offset = a + b\theta \quad \text{A5}$$

And *a* and *b* are empirically calculated coefficients and θ is the satellite zenith angle.

If

$$SI_{bennarts} > 10 \quad \text{A6}$$

Then the field of view is flagged as rain.

Current operational values for the coefficients are

AMSU-B: *a*=-35.6, *b*=0.139

SSMIS: *a*=-35.6, *b*=0.130

Default: *a*=-32.956, *b*=0.164

A1.3 Cirrus cost test ('mwbcloudy' flag)

Cost function *J* is calculated from the 183.31+/-7 GHz, 183.31+/-3 GHz and 183.31+/-1 GHz channels using equation A7.

$$J = \frac{1}{2} dT \left[H(d) B H(d)^T + R \right]^{-1} d \qquad \text{A7}$$

d = *O-B*

H is the tangent linear operator

B is the Background error covariance matrix

R is the observation + forward model error covariance matrix

If J is greater than 0.058 and the difference between observed and

background BT for 183.31+/-7 GHz is greater than 2 K then the field of view is flagged as cloudy.

Source Sreerekha et al 2008 (EUMETSAT Contract EUM/CO/07/4600000409/CJA)

A1.4 AAPP Surface test ('mwcloudy' flag)

The surface test estimates surface type and flags an observation if deep cloud liquid water is suspected.

A minimum variance scheme is used, as shown in equation A8

$$J = \left(BT - BT_{mean} \right) C^{-1} \left(BT - BT_{mean} \right)^{-1} \qquad \text{A8}$$

where

BT is the vector of observed brightness temperatures

BT_{mean} is the vector of mean brightness temperatures calculated by the radiative transfer model assuming no cloud liquid water.

C is the covariance matrix of the brightness temperature

BT_{mean} and *C* are calculated for the 20 AMSU channels for 9 surface types and assuming no cloud liquid water.

The surface type which minimises *J* is assigned to the field of view

If surface selected is sea and if *J* is greater than a threshold then cloud liquid water flag is set.

Currently AMSU channels 1, 2 and 3 are used.

Eight surface types are determined:

1 = Bare young ice (i.e. new ice, no snow)

2 = Dry land (i.e. dry with or without significant vegetation)

3 = Dry snow (i.e. snow with water less than 2%, over land)

4 = Multi-year ice (i.e. old ice with snow [assumed dry] cover)

5 = Sea (i.e. open water, no islands, ice-free, wind < 14 m/s)

6 = Wet forest (i.e. established forest with wet canopy)

7 = Wet land (i.e. non-forested land with a wet surface)

8 = Wet snow (i.e. snow with water content > 2%)

Note : If surface type is 1, 4 or 8 and channel 1 > 275 K surface type is set to

9 = Desert.

Source AAPP Science document
(http://research.metoffice.gov.uk/research/interproj/nwpsaf/aapp/index.html)

[i] http://mirs.nesdis.noaa.gov/npoessatms.php
[ii] http://research.metoffice.gov.uk/research/interproj/nwpsaf/aapp/index.html
[iii] http://cimss.ssec.wisc.edu/cspp/

Met Office
FitzRoy Road, Exeter
Devon EX1 3PB
United Kingdom

Tel: 0870 900 0100
Fax: 0870 900 5050
enquiries@metoffice.gov.uk
www.metoffice.gov.uk